

Z' -induced FCNC decays of top, beauty and strange quarks

Kaori Fuyuto^a, Wei-Shu Hou^b, and Masaya Kohda^c

^a*Department of Physics, Nagoya University, Nagoya 464-8602, Japan*

^b*Department of Physics, National Taiwan University, Taipei 10617, Taiwan*

^c*Department of Physics, Chung-Yuan Christian University, Chung-Li 32023, Taiwan*

Anomalous $b \rightarrow s$ transitions from LHCb data may suggest a new massive gauge boson Z' that couples to the left-handed $b \rightarrow s$ current, which in turn implies a coupling to the $t \rightarrow c$ current. In this paper, we study flavor-changing neutral current (FCNC) decays of the top quark induced by a Z' boson, namely $t \rightarrow cZ'$, based on a model of the gauged $L_\mu - L_\tau$ symmetry (the difference between the muon and tauon numbers) with vector-like quarks, which was introduced to explain the anomalous LHCb data. We illustrate that searching for $t \rightarrow cZ'$ via $Z' \rightarrow \mu^+\mu^-$ with LHC Run 1 data can already probe a parameter region which is unexplored by B physics for the Z' mass around $\mathcal{O}(10)$ GeV or more. We further extend the model to very light Z' with mass below 400 MeV, which is motivated by the muon $g - 2$ anomaly. Taking rare B and K meson decay data into account, we give upper limits on the $t \rightarrow cZ'$ branching ratio for the light Z' case, and discuss about its observability at the LHC. We also scrutinize the possibility that the decay $K_L \rightarrow \pi^0 Z'$ with $Z' \rightarrow \nu\bar{\nu}$ may lead to apparent violation of the usual Grossman–Nir bound of $\mathcal{B}(K_L \rightarrow \pi^0 \nu\bar{\nu}) < 1.4 \times 10^{-9}$.

PACS numbers: 13.20.Eb 13.20.He 14.65.Ha 14.70.Pw

I. INTRODUCTION

Measuring top quark properties is one of the major tasks at the Large Hadron Collider (LHC). In particular, the large amount of $t\bar{t}$ events enables the search for exotic decay modes of the top quark. In line with this, top quark decays via flavor-changing neutral currents (FCNCs) by emitting the Standard Model (SM) gauge bosons or the Higgs boson have been under intense study by the ATLAS and CMS experiments [1]. Furthermore, top quark decays offer opportunities to directly search for New Physics, e.g. a charged Higgs boson (H^\pm) in $t \rightarrow bH^\pm$ decay [1].

For the down-sector counterpart, the decay properties of bottom quarks, i.e. B mesons, have been investigated thoroughly in the last three decades. So far, there are no significant deviations from SM in the vast amount of B factory and LHC data. From LHC Run 1 data, however, the LHCb experiment has found two tantalizing hints for New Physics beyond SM (BSM) in $b \rightarrow s$ transitions. One is the $\sim 3\sigma$ tension with SM in the angular analysis of $B^0 \rightarrow K^{*0}\mu^+\mu^-$ decay, namely the P'_5 anomaly [2, 3]. The other is a violation of lepton flavor universality observed in $B^+ \rightarrow K^+\ell^+\ell^-$ ($\ell = e$ or μ) decay rates, indicating a 2.6σ discrepancy from the SM prediction, i.e. the R_K anomaly [4]. Although these may be due to statistical fluctuations and/or underestimated hadronic uncertainties, model-independent studies for possible BSM effects have revealed that both the P'_5 [5–9] and R_K [10–12] anomalies can be better explained by adding a new contribution to C_9^μ , the Wilson coefficient of the effective operator $(\bar{s}_L\gamma_\alpha b_L)(\bar{\mu}\gamma^\alpha\mu)$. Surprisingly, the required amount of New Physics contribution to C_9^μ for the two anomalies is similar [13, 14].

The extra contribution to C_9^μ can be generated by a new massive gauge boson Z' that couples to the muon vector current. In Ref. [15], a Z' model was constructed based on the gauged $L_\mu - L_\tau$ symmetry [16], the dif-

ference between the muon and tauon numbers. As an effective theory, the model permits Z' couplings to the SM quark currents through [17] higher dimensional operators. Ref. [15] gave a viable UV-complete model by introducing new vector-like quarks which mix with SM quarks. The model predicts an effective tcZ' coupling on the same footing, leading to $t \rightarrow cZ'$ decay if the Z' is lighter than the top. Such a light Z' is allowed, as it is well hidden with no direct couplings to SM particles, except the muon, tau and the associated neutrinos. The $t \rightarrow cZ'$ decay, followed by $Z' \rightarrow \mu^+\mu^-/\tau^+\tau^-$, opens up a new window to search for the Z' [18].

Another phenomenological motivation to introduce the gauged $L_\mu - L_\tau$ symmetry comes from the long-standing $\sim 3\sigma$ discrepancy in the muon anomalous magnetic moment $a_\mu \equiv (g_\mu - 2)/2$ between experimental data and SM predictions [19]. The radiative correction by the Z' loop can provide [20] the right amount of shift, $\Delta a_\mu \sim 3 \times 10^{-9}$, to match with data. It was found [21] recently, however, that the Z' effect is severely constrained by the neutrino trident production $\nu_\mu N \rightarrow \nu_\mu N \mu^+\mu^-$ process: the good agreement between experimental data and SM prediction excludes a large portion of the parameter region that could explain the muon $g - 2$ anomaly, leaving only the rather *light* Z' case,

$$m_{Z'} \lesssim 400 \text{ MeV} \quad (\text{muon } g - 2). \quad (1)$$

Given this constraint, the muon $g - 2$ anomaly and the $b \rightarrow s$ transition anomalies cannot be explained simultaneously, as the latter requires a *heavy* Z' with mass suitably above m_b to generate the contact $(\bar{s}b)(\bar{\mu}\mu)$ interaction for C_9^μ . But it is still interesting to investigate connections with the quark currents even for the light Z' case that satisfies Eq. (1): the $t \rightarrow cZ'$ decay, followed by $Z' \rightarrow \mu^+\mu^-$, would exhibit the interesting collider signature of collimated opposite-sign muons from a highly boosted Z' . Moreover, the mass range of Eq. (1) implies that the Z' can be directly produced in B and K meson

decays. We have pointed out in Ref. [22] that such a Z' with mass around m_{π^0} can evade $K^+ \rightarrow \pi^+ Z'$ searches, but cause $K_L \rightarrow \pi^0 Z'$ ($\rightarrow \nu\bar{\nu}$) with rate exceeding the commonly perceived Grossman–Nir (GN) bound [23] of $\mathcal{B}(K_L \rightarrow \pi^0 \nu\bar{\nu}) < 1.4 \times 10^{-9}$. Note that a very light Z' of $L_\mu - L_\tau$ might explain [24] the PeV-scale cosmic neutrino spectrum observed by IceCube [25].

In this paper, we investigate how large the $t \rightarrow cZ'$ decay rate can be,¹ based on the gauged $L_\mu - L_\tau$ model of Ref. [15]. We consider the two well-motivated Z' mass ranges: (i) the heavy Z' scenario with $m_b \lesssim m_{Z'} < m_t - m_c$, which is motivated by the P'_5 and R_K anomalies; (ii) the light Z' scenario with $m_{Z'} \lesssim 400$ MeV, which is motivated by the muon $g - 2$ anomaly. The former was already sketched in Ref. [15]. It was pointed out that the right-handed tcZ' coupling is unconstrained from B and K meson data and can lead to the $t \rightarrow cZ'$ decay with $\sim 1\%$ branching ratio. We revisit their result by updating $b \rightarrow s$ transition data with a correction to the $t \rightarrow cZ'$ formula. On the other hand, Scenario (ii) was not studied in Ref. [15], but clearly exhibits rather different phenomenology compared to Scenario (i). As the on-shell Z' could be produced by B and K meson decays, the meson decay rates could be hugely enhanced, and even the right-handed tcZ' coupling is constrained by data at one-loop level. Scenario (ii) is further divided into two categories: (ii-a) $2m_\mu < m_{Z'} \lesssim 400$ MeV; (ii-b) $m_{Z'} < 2m_\mu$. In Scenario (ii-b), the Z' decays only into neutrinos, rendering $t \rightarrow cZ'$ searches at the LHC difficult, but it gives interesting implications for rare kaon decays as mentioned above.

This paper is organized as follows. We recapitulate in Sec. II the model of Ref. [15], then study $t \rightarrow cZ'$ in Scenario (i) for heavy Z' motivated by the $b \rightarrow s$ anomalies. We then discuss the observability of $t \rightarrow cZ'$ decay at the LHC with $Z' \rightarrow \mu^+ \mu^-$. In Sec. III and IV, we study $t \rightarrow cZ'$ for light Z' motivated by the muon $g - 2$ anomaly. We consider Scenario (ii-a) in Sec. III, where the Z' mass is above dimuon threshold. We give formulas for FCNC B and K decays, collect relevant rare B and K decay data, then give upper limits on $t \rightarrow cZ'$ branching ratio. In Sec. IV, we consider Scenario (ii-b) where the Z' is below the dimuon threshold. After giving upper limits on $t \rightarrow cZ'$ branching ratios, we discuss a special implication for rare kaon decay experiments, expanding the discussion of Ref. [22]. Sec. V is devoted to discussion and conclusions. In Appendix A, we give the decay distribution for $B^0 \rightarrow K^{*0} Z' \rightarrow K \pi \mu^+ \mu^-$ four-body decay to estimate the efficiency at LHCb. In Appendix B, loop functions used in our analysis are given.

II. P'_5 - AND R_K -MOTIVATED Z'

A. Model

We first recapitulate the model introduced in Ref. [15]. A new Abelian gauge group $U(1)'$ is introduced that gauges the $L_\mu - L_\tau$ symmetry. This $U(1)'$ symmetry is spontaneously broken by the vacuum expectation value (v.e.v.) of a scalar field Φ , which is charged under $U(1)'$ but singlet under the SM gauge group. The mass of Z' is given then by $m_{Z'} = g' v_\Phi$, where g' is the $U(1)'$ gauge coupling and $v_\Phi = \sqrt{2} \langle \Phi \rangle$ is the v.e.v. of Φ . We adopt the convention where the covariant derivative acting on Φ is given by $D_\alpha = \partial_\alpha + ig' \mathcal{Q}'_\Phi Z'_\alpha$, with $\mathcal{Q}'_\Phi = +1$ the $U(1)'$ charge of Φ . The Z' couples to leptons via

$$\mathcal{L} \supset -g' Z'_\alpha (\bar{\mu} \gamma^\alpha \mu + \bar{\nu}_{\mu L} \gamma^\alpha \nu_{\mu L} - \bar{\tau} \gamma^\alpha \tau - \bar{\nu}_{\tau L} \gamma^\alpha \nu_{\tau L}). \quad (2)$$

We set the kinetic mixing between the $U(1)'$ and $U(1)_Y$ gauge bosons to be zero throughout this paper.

In order to induce the effective Z' couplings to the SM quark currents, new vector-like quarks, which mix with the SM quarks, are introduced: $Q_L = (U_L, D_L)$, U_R, D_R , which replicates one generation of SM quarks, and chiral partners $\tilde{Q}_R = (\tilde{U}_R, \tilde{D}_R)$, \tilde{U}_L, \tilde{D}_L . Unlike the SM quarks, the new vector-like quarks are charged under $U(1)'$, with charges $\mathcal{Q}'_Q = +1$ for $Q \equiv Q_L + \tilde{Q}_R$ and $\mathcal{Q}'_U = \mathcal{Q}'_D = -1$ for $U \equiv \tilde{U}_L + U_R$ and $D \equiv \tilde{D}_L + D_R$. The mass term for the vector-like quarks is given by

$$-\mathcal{L}_m = m_Q \bar{Q} Q + m_U \bar{U} U + m_D \bar{D} D, \quad (3)$$

where the three mass parameters are taken to be real without loss of generality. The Yukawa mixing term between the vector-like quarks and SM quarks is given by

$$-\mathcal{L}_{\text{mix}} = \Phi \sum_{i=1}^3 \left(\tilde{U}_R Y_{Q u_i} u_{iL} + \tilde{D}_R Y_{Q d_i} d_{iL} \right) + \Phi^\dagger \sum_{i=1}^3 \left(\tilde{U}_L Y_{U u_i} u_{iR} + \tilde{D}_L Y_{D d_i} d_{iR} \right) + \text{h.c.} \quad (4)$$

Here, $SU(2)_L$ symmetry imposes

$$Y_{Q u_i} = \sum_{j=1}^3 V_{u_i d_j}^* Y_{Q d_j}, \quad (5)$$

for $i = 1, 2, 3$, where $V_{u_i d_j}$ is an element of the Cabibbo-Kobayashi-Maskawa (CKM) matrix.

Integrating out the heavy vector-like quarks, one obtains the effective Z' couplings to the SM quarks as

$$\mathcal{L}_{\text{eff}} \supset -Z'_\alpha \sum_{i,j=1}^3 \left(g_{u_i u_j}^L \bar{u}_{iL} \gamma^\alpha u_{jL} + g_{u_i u_j}^R \bar{u}_{iR} \gamma^\alpha u_{jR} + g_{d_i d_j}^L \bar{d}_{iL} \gamma^\alpha d_{jL} + g_{d_i d_j}^R \bar{d}_{iR} \gamma^\alpha d_{jR} \right), \quad (6)$$

¹ Due to constraints from D meson mixing and decay data, $t \rightarrow cZ'$ and $t \rightarrow uZ'$ cannot be simultaneously large. We concentrate on possibilities for large $t \rightarrow cZ'$ rates in this paper.

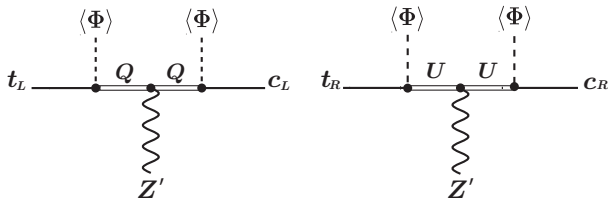


FIG. 1. Diagrams that induce effective tcZ' couplings.

where

$$g_{u_i u_j}^L = +g' \frac{Y_{Q u_i}^* Y_{Q u_j} v_\Phi^2}{2m_Q^2}, \quad g_{u_i u_j}^R = -g' \frac{Y_{U u_i}^* Y_{U u_j} v_\Phi^2}{2m_U^2},$$

$$g_{d_i d_j}^L = +g' \frac{Y_{Q d_i}^* Y_{Q d_j} v_\Phi^2}{2m_Q^2}, \quad g_{d_i d_j}^R = -g' \frac{Y_{D d_i}^* Y_{D d_j} v_\Phi^2}{2m_D^2}. \quad (7)$$

The effective couplings to $t \rightarrow c$ currents, for instance, are generated by the diagrams shown in Fig. 1.

After integrating out Q, U, D , the Yukawa mixing couplings in Eq. (4) induce also the effective couplings of Φ to the SM quark bilinears. In particular, the physical mode of the Φ field, ϕ , may couple to the top and charm quarks, hence the top FCNC decay $t \rightarrow c\phi$ can occur, if the ϕ boson is lighter than the top. In this paper, we concentrate on the decay $t \rightarrow cZ'$, assuming that the ϕ is heavier than the top. Phenomenology of the $U(1)'$ Higgs boson ϕ will be investigated elsewhere [26].

B. P'_5 and R_K anomalies

The effective bsZ' couplings in Eq. (7), in combination with Eq. (2), induce extra contributions to $b \rightarrow s\mu^+\mu^-$ decays. Assuming the Z' is heavy compared to the B meson mass scale, one may integrate out the Z' and obtain BSM contributions to the $b \rightarrow s$ effective Hamiltonian

$$\Delta C_9^\mu (\bar{s}\gamma_\alpha P_L b)(\bar{\mu}\gamma^\alpha \mu) + C_9^{\prime\mu} (\bar{s}\gamma_\alpha P_R b)(\bar{\mu}\gamma^\alpha \mu), \quad (8)$$

with the Wilson coefficients

$$\Delta C_9^\mu \simeq +\frac{Y_{Qs}^* Y_{Qb}}{2m_Q^2}, \quad C_9^{\prime\mu} \simeq -\frac{Y_{Ds}^* Y_{Db}}{2m_D^2}, \quad (9)$$

where g' and v_Φ cancel out in the final expressions. Note that the electron counterparts are unchanged, i.e. $\Delta C_9^e = C_9^{\prime e} = 0$, resulting in the violation of lepton flavor universality in $b \rightarrow s\ell^+\ell^-$ between $\ell = \mu, e$.

In Ref. [15], the values $\Delta C_9^\mu \simeq -(35 \text{ TeV})^{-2}$, $C_9^{\prime\mu} \simeq +(35 \text{ TeV})^{-2}$ from a global analysis [6] of $b \rightarrow s$ data was adopted as a solution for the P'_5 anomaly [2]. Since then, the R_K anomaly [4] has emerged, while P'_5 has been updated with the 3 fb^{-1} dataset by LHCb [3]. A recent global analysis [14], after the P'_5 update, found the best fit values $\Delta C_9^\mu \simeq -(34 \text{ TeV})^{-2}$, $C_9^{\prime\mu} \simeq +(54 \text{ TeV})^{-2}$. We remark that this fit does not include $b \rightarrow se^+e^-$ modes, while R_K is defined by the ratio $R_K \equiv \mathcal{B}(B^+ \rightarrow$

$K^+\mu^+\mu^-)/\mathcal{B}(B^+ \rightarrow K^+e^+e^-)$. The measured R_K value [4] is better explained by $C_9^{\prime\mu} \sim 0$ with a ΔC_9^μ value similar to the above best fit value, which is still within the 1σ ellipse of the allowed region in Ref. [14]. For illustration, therefore, we take the following values as a reference point to solve the $b \rightarrow s$ anomalies:

$$\Delta C_9^\mu \simeq -(34 \text{ TeV})^{-2}, \quad C_9^{\prime\mu} \sim 0. \quad (10)$$

Interpreted within the Z' model, the values of Eq. (10) correspond to ²

$$m_Q \simeq 24 \text{ TeV} \times (-Y_{Qb} Y_{Qs}^*)^{1/2}, \quad (11)$$

with real and negative $Y_{Qb} Y_{Qs}^*$, and $Y_{Db} Y_{Ds}^*/m_D^2 \sim 0$. The latter implies the vector-like quark D is decoupled. For hierarchical Yukawa couplings, $Y_{Qb} = 1$, $Y_{Qs} = -\lambda^2$ with $\lambda \simeq 0.23$, Eq. (11) implies $m_Q \simeq 5.5 \text{ TeV}$.

C. Constraints on v_Φ

Before entering the discussion on the $t \rightarrow cZ'$ decay, we summarize constraints on v_Φ , the v.e.v. of the $U(1)'$ Higgs field, which is of great importance to $t \rightarrow cZ'$.

The most significant constraint comes from neutrino trident production, i.e. $\nu_\mu N \rightarrow \nu_\mu N \mu^+ \mu^-$, with the normalized cross section [15]

$$\frac{\sigma}{\sigma_{\text{SM}}} \simeq \frac{1 + (1 + 4s_W^2 + 2v^2/v_\Phi^2)^2}{1 + (1 + 4s_W^2)^2}, \quad (12)$$

for heavy Z' . Using CCFR data [27], which imply $\sigma_{\text{exp}}/\sigma_{\text{SM}} = 0.82 \pm 0.28$, we obtain the 2σ lower bound

$$v_\Phi \gtrsim 540 \text{ GeV for } m_{Z'} \gtrsim 10 \text{ GeV}. \quad (13)$$

For a fixed $m_{Z'}$, this constraint can be translated into an upper bound on $g' = m_{Z'}/v_\Phi$, i.e., $g' \lesssim 0.09 \times (m_{Z'}/50 \text{ GeV})$. For $m_{Z'} \lesssim 10 \text{ GeV}$, the constraint is softened [21], as we will see in the next section.

For Z' lighter than the Z boson, the coupling g' is also constrained by $Z \rightarrow 4\ell$ searches at the LHC. An analysis [15, 21] that utilizes the Run 1 result of ATLAS [28] found that the $Z \rightarrow 4\ell$ [29] provides slightly tighter constraints than the neutrino trident production for $9 \text{ GeV} \lesssim m_{Z'} \lesssim 50 \text{ GeV}$. The strongest bound $g' \lesssim 0.01$ is attained for $m_{Z'} \sim 10 \text{ GeV}$, leading to $v_\Phi \gtrsim 1000 \text{ GeV}$ around this mass value. This loses sensitivity for lower Z' masses due to the cut applied in the experimental analysis.

For $m_{Z'} \gg m_\mu$, the Z' contribution to muon $g-2$ is given by $\Delta a_\mu \simeq m_\mu^2/(12\pi^2 v_\Phi^2)$ [20]. To explain the discrepancy between experiment and theory, $\Delta a_\mu = (2.9 \pm 0.9) \times 10^{-9}$ [19], one needs $160 \text{ GeV} \lesssim v_\Phi \lesssim 220$

² Note that the sign for $Y_{Qb} Y_{Qs}^*$ is opposite the one in Ref. [15].

GeV. This range is excluded by the constraint from the neutrino trident production, Eq. (13). The case for the light Z' will be discussed in the next section.

The effective bsZ' coupling induces B_s mixing, which provides an upper bound on v_Φ . The modification to the B_s mixing amplitude is given by [15]

$$\frac{M_{12}}{M_{12}^{\text{SM}}} \simeq 1 + (Y_{Qb}Y_{Qs}^*)^2 \left(\frac{v_\Phi^2}{m_Q^4} + \frac{1}{16\pi^2} \frac{1}{m_Q^2} \right) \times \left[\frac{g_2^4}{16\pi^2} \frac{1}{m_W^2} (V_{ts}^* V_{tb})^2 S_0 \right]^{-1}, \quad (14)$$

where $S_0 \simeq 2.3$ and the D quark effects are decoupled, given the $b \rightarrow s$ transition data. It is useful to eliminate [30] the dependence on $Y_{Qb}Y_{Qs}^*/m_Q^2$ in terms of ΔC_9^μ of Eq. (9). Then, allowing BSM effects up to 15% [15], we find the upper bound

$$v_\Phi \lesssim 5.6 \text{ TeV} \left(\frac{(34 \text{ TeV})^{-2}}{|\Delta C_9^\mu|} \right). \quad (15)$$

We have neglected the $1/m_Q^2$ term in Eq. (14), which is numerically valid for $m_Q \lesssim 10$ TeV. For larger m_Q , the bound gets gradually stronger, e.g. $v_\Phi \lesssim 5.4$ (3.9) TeV for $m_Q = 20$ (50) TeV, with ΔC_9^μ satisfying Eq. (10).

The constraint from kaon mixing can be avoided by assuming the mixing of Q and D quarks with d quark is suppressed: $Y_{Qd} \simeq Y_{Dd} \simeq 0$. Although this assumption leads to $Y_{Qu} \simeq \lambda Y_{Qs}$ via Eq. (5), hence a new contribution to D mixing, B_s mixing still gives the strongest constraint [15]. We further set $Y_{Uu} \simeq 0$ to switch off the right-handed $c \rightarrow u$ current contribution to D mixing, in order to pursue the possibility of large $t \rightarrow cZ'$ rate.

D. Branching ratio for $t \rightarrow cZ'$

We now turn to $t \rightarrow cZ'$ decay. With the effective tcZ' couplings in Eq. (7), the decay rate is given by

$$\Gamma(t \rightarrow cZ') = \frac{m_t}{32\pi} \lambda^{1/2}(1, x_c, x') \left[(|g_{ct}^L|^2 + |g_{ct}^R|^2) [1 + x_c - 2x' + (1 - x_c)^2/x'] - 12\text{Re}(g_{ct}^R g_{ct}^{L*}) \sqrt{x_c} \right], \quad (16)$$

where $x_c \equiv m_c^2/m_t^2$, $x' \equiv m_{Z'}^2/m_t^2$ and

$$\lambda(x, y, z) \equiv x^2 + y^2 + z^2 - 2(xy + yz + zx). \quad (17)$$

Taking the ratio with the $t \rightarrow bW$ rate, the $t \rightarrow cZ'$ branching ratio is given by

$$\mathcal{B}(t \rightarrow cZ') \simeq \frac{(1 - x')^2(1 + 2x')}{2(1 - x_W)^2(1 + 2x_W)} \times \left(|Y_{Qt}Y_{Qc}^*|^2 \frac{v^2 v_\Phi^2}{4m_Q^4} + |Y_{Ut}Y_{Uc}^*|^2 \frac{v^2 v_\Phi^2}{4m_U^4} \right), \quad (18)$$

where $x_W \equiv m_W^2/m_t^2$, and we have set m_c^2/m_t^2 , $m_b^2/m_t^2 \rightarrow 0$. Note that our result is a factor of four smaller than the one shown in Ref. [15].

The first term in Eq. (18) is induced by the left-handed $t \rightarrow c$ current (first diagram in Fig. 1), which is related to the left-handed $b \rightarrow s$ current by $SU(2)_L$ symmetry. Neglecting Cabibbo suppressed terms, Eq. (5) implies $Y_{Qt} \sim Y_{Qb}$, $Y_{Qc} \sim Y_{Qs}$. One may eliminate the $Y_{Qt}Y_{Qc}^*/m_Q^2$ dependence in Eq. (18) by using ΔC_9^μ [Eq. (9)] to rewrite the left-handed current contribution

$$\mathcal{B}(t \rightarrow cZ')_{\text{LH}} \simeq \frac{(1 - x')^2(1 + 2x')}{2(1 - x_W)^2(1 + 2x_W)} |\Delta C_9^\mu|^2 v^2 v_\Phi^2. \quad (19)$$

Applying the lower bound, Eq. (13), and upper bound, Eq. (15), on v_Φ , we obtain the allowed range for left-handed current contribution:

$$0.7 \times 10^{-8} \lesssim \mathcal{B}(t \rightarrow cZ')_{\text{LH}} \lesssim 0.8 \times 10^{-6}, \quad (20)$$

for a Z' mass sufficiently below the kinematic threshold. Note that the lower limit assumes the central value of ΔC_9^μ from the global fit in Eq. (10), while the upper limit is insensitive to ΔC_9^μ as the dependence cancels out. The branching ratio can be slightly larger than the upper value quoted in Ref. [15], i.e. $\text{few} \times 10^{-7}$. This is because the B_s -mixing constraint on v_Φ , Eq. (15), is weakened due to the decoupling of D quark effects, which is favored by the measured R_K value.

On the other hand, the second term in Eq. (18), induced by the right-handed $t \rightarrow c$ current (second diagram in Fig. 1), is not related to FCNCs in the down-type quark sector. Treating m_U , Y_{Ut} and Y_{Uc} as free parameters, the right-handed current contribution can be easily enhanced over the left-handed current contribution. To see how large it can be, we introduce a mixing parameter between the vector-like quark U and t_R or c_R as

$$\delta_{Uq} \equiv \frac{Y_{Uq} v_\Phi}{\sqrt{2} m_U}, \quad (q = t, c) \quad (21)$$

and recast the right-handed current contribution as

$$\mathcal{B}(t \rightarrow cZ')_{\text{RH}} \simeq \frac{(1 - x')^2(1 + 2x')}{2(1 - x_W)^2(1 + 2x_W)} \frac{v^2}{v_\Phi^2} |\delta_{Ut} \delta_{Uc}^*|^2. \quad (22)$$

For fixed values of δ_{Ut} and δ_{Uc} , this can be enhanced by lowering the value of v_Φ , which is bounded from below by neutrino trident production [Eq. (13)]. Taking reasonably large mixing parameters $\delta_{Ut} = \delta_{Uc} \simeq \lambda$ for illustration, Eq. (13) implies

$$\mathcal{B}(t \rightarrow cZ')_{\text{RH}} \lesssim 3 \times 10^{-4} \quad (\delta_{Ut} = \delta_{Uc} \simeq \lambda). \quad (23)$$

This is smaller than the value in Ref. [15], i.e. $\sim 1\%$, partially because of the correction factor $1/4$ in Eq. (18). In the corrected formula, the $\sim 1\%$ branching ratio requires rather large mixing parameters: $\delta_{Ut} \sim \delta_{Uc} \sim 0.5$.

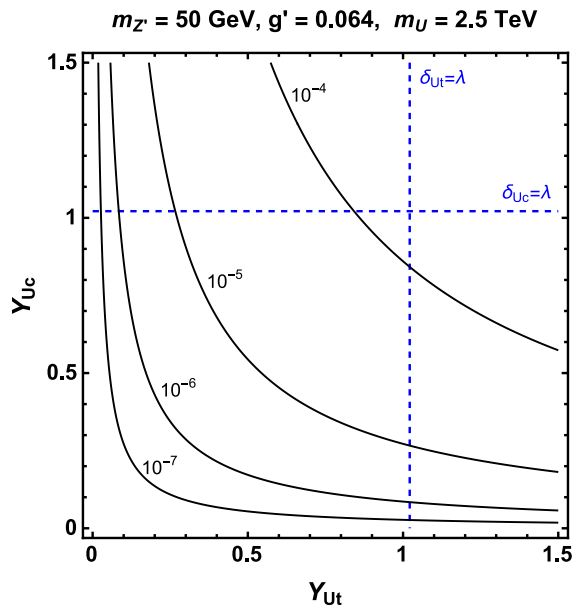


FIG. 2. Contours for $\mathcal{B}(t \rightarrow cZ')_{\text{RH}}$ in the (Y_{Ut}, Y_{Uc}) plane for $m_{Z'} = 50$ GeV, $g' = 0.064$, $v_\Phi = 780$ GeV, and $m_U = 2.5$ TeV. In estimating $\mathcal{B}(t \rightarrow cZ')$, only the contribution from second term in Eq. (18), i.e. right-handed $t \rightarrow c$ current, is included. The vertical (horizontal) blue dashed line marks the value of Y_{Ut} (Y_{Uc}) above which the mixing parameter δ_{Ut} (δ_{Uc}) exceeds $\lambda \simeq 0.23$.

In Fig. 2, contours of $\mathcal{B}(t \rightarrow cZ')_{\text{RH}}$ are given in the (Y_{Ut}, Y_{Uc}) plane for $m_{Z'} = 50$ GeV, $g' = 0.064$, $v_\Phi = 780$ GeV, and $m_U = 2.5$ TeV. The vertical (horizontal) dashed lines mark the value of Y_{Ut} (Y_{Uc}) above which the mixing parameter δ_{Ut} (δ_{Uc}) exceeds λ . These lines are placed as a rough indication for reasonable range of Yukawa mixing couplings Y_{Uq} . The figure illustrates that $\mathcal{B}(t \rightarrow cZ')_{\text{RH}}$ can exceed 10^{-4} for $Y_{Ut}, Y_{Uc} \sim 1$, with $\delta_{Ut}, \delta_{Uc} < \lambda$ satisfied.

Before turning to search at LHC, we give the partial widths for Z' decay

$$\begin{aligned} \Gamma(Z' \rightarrow \ell^+ \ell^-) &= \frac{g'^2}{12\pi} m_{Z'} \left[1 - \frac{4m_\ell^2}{m_{Z'}^2} \right]^{\frac{1}{2}} \left[1 + \frac{2m_\ell^2}{m_{Z'}^2} \right], \\ \Gamma(Z' \rightarrow \nu_\ell \bar{\nu}_\ell) &= \frac{g'^2}{24\pi} m_{Z'}, \end{aligned} \quad (24)$$

where $\ell = \mu, \tau$. The approximate branching ratios are

$$\begin{aligned} \mathcal{B}_{\tau\tau} &\simeq \mathcal{B}_{\mu\mu} \simeq \mathcal{B}_{\nu\nu} \simeq \frac{1}{3} \quad (2m_\tau \ll m_{Z'}), \\ \mathcal{B}_{\mu\mu} &\simeq \mathcal{B}_{\nu\nu} \simeq \frac{1}{2} \quad (2m_\mu \ll m_{Z'} < 2m_\tau), \\ \mathcal{B}_{\nu\nu} &= 1 \quad (m_{Z'} < 2m_\mu). \end{aligned} \quad (25)$$

E. $t \rightarrow cZ'$ search at LHC

The decay $t \rightarrow cZ'$ followed by $Z' \rightarrow \ell^+ \ell^-$ ($\ell = \mu, \tau$) can be searched for in $t\bar{t}$ events at the LHC. It is similar

to $t \rightarrow qZ$ ($q = u, c$) decay, which has been searched for by the ATLAS [31] and CMS [32] experiments using $t\bar{t} \rightarrow Zq + Wb$ with leptonically decaying Z and W , resulting in a final state with three charged leptons. The $t \rightarrow cZ'$ decay with heavy Z' should be searched for in an analogous way, by modifying event selection criteria for an opposite sign charged lepton pair.

The current best limit on the $t \rightarrow qZ$ rate comes from the CMS analysis with the full Run 1 dataset [32], finding $\mathcal{B}(t \rightarrow qZ) < 5 \times 10^{-4}$ at 95% C.L., while the ATLAS [31], based on the 20.3 fb^{-1} dataset of the 8 TeV run, found $\mathcal{B}(t \rightarrow qZ) < 7 \times 10^{-4}$ at 95% C.L. These limits should be improved with more data during the 13/14 TeV run of the LHC. The expected limits at the 14 TeV LHC with 300 fb^{-1} (3000 fb^{-1}) data are $\mathcal{B}(t \rightarrow qZ) < 2.7 \times 10^{-4}$ (1.0×10^{-4}) for CMS [33],³ and $\mathcal{B}(t \rightarrow qZ) < 2.2 \times 10^{-4}$ (7×10^{-5}) for ATLAS [36, 37].

For illustration, we attempt a reinterpretation of the CMS limits for $t \rightarrow cZ$ to the case for $t \rightarrow cZ'$ by a simple scaling of Z and Z' decay branching ratios into the charged leptons ($\ell = e, \mu$). An advantage of the $t \rightarrow cZ'$ search is the larger Z' branching ratio, e.g., $\mathcal{B}(Z' \rightarrow \mu^+ \mu^-) \simeq 1/3$ for $m_{Z'} \gg 2m_\tau$, compared with $\mathcal{B}(Z \rightarrow \ell^+ \ell^-) \simeq 0.07$ (summed over e and μ). Multiplying the factor of $\mathcal{B}(Z \rightarrow \ell^+ \ell^-)/\mathcal{B}(Z' \rightarrow \ell^+ \ell^-) \simeq 0.2$ to the current [32] and future [33] CMS limits for $t \rightarrow cZ$, we infer sensitivities for $t \rightarrow cZ' (\rightarrow \mu^+ \mu^-)$ by CMS as

$$\mathcal{B}(t \rightarrow cZ') \lesssim \begin{cases} 10^{-4} & (\text{“CMS” Run 1}), \\ 5 \times 10^{-5} & (\text{“CMS” } 300 \text{ fb}^{-1}), \\ 2 \times 10^{-5} & (\text{“CMS” } 3000 \text{ fb}^{-1}) \end{cases} \quad (26)$$

for the heavy Z' with $m_{Z'} \sim \mathcal{O}(10)$ GeV. The scaling of the ATLAS limits gives similar results. Therefore, the right-handed current induced $t \rightarrow cZ'$ might already be probed by Run 1 data (see Fig. 2), while the left-handed current contribution seems to be beyond the sensitivity of LHC, even with 3000 fb^{-1} data [see Eq. (20)].

For light Z' with $2m_\mu < m_{Z'} \lesssim 400$ MeV, the scaling factor is slightly reduced as $\mathcal{B}(Z \rightarrow \ell^+ \ell^-)/\mathcal{B}(Z' \rightarrow \ell^+ \ell^-) \simeq 0.14$ due to larger $Z' \rightarrow \mu^+ \mu^-$ branching ratio ($\simeq 1/2$). For such a light Z' , however, the search strategy needs to be changed. In particular, muon pairs produced by boosted Z' bosons would be highly collimated, while the existing $t \rightarrow qZ$ search requires events with isolated charged leptons. Nevertheless, we adopt Eq. (26) for the light Z' case as target values in the following analysis.

For the light Z' with $m_{Z'} < 2m_\mu$, the Z' decays only into neutrino pairs. Thus, the search at the LHC would be quite challenging.⁴

³ In the Snowmass White Paper [34], a more optimistic value $\sim 10^{-5}$ is quoted as the CMS sensitivity for $t \rightarrow qZ$ with 300 fb^{-1} data at the 14 TeV LHC. This was based on extrapolating from the 7 TeV result [35]. The projections in Ref. [33], on the other hand, are based on Monte Carlo analysis.

⁴ The $t \rightarrow q$ ($q = u, c$) decay with missing energy has been discussed based on dark matter models [38, 39].

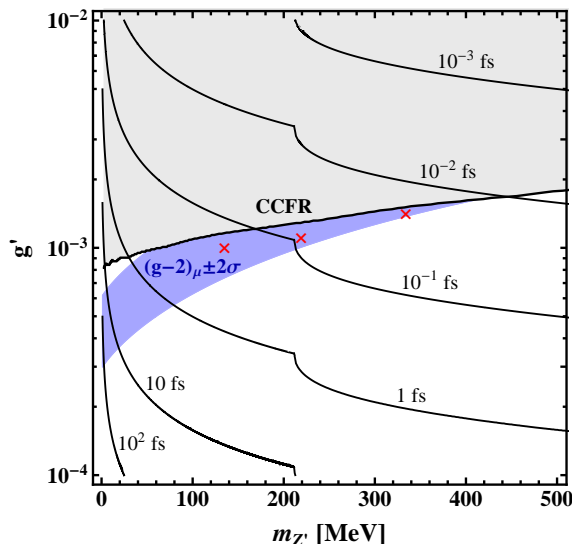


FIG. 3. Lifetime of light Z' with relevant constraints in the $(m_{Z'}, g')$ plane: solid lines are labeled contours for $\tau_{Z'}$, the blue-shaded band is the region favored by muon $g-2$ within 2σ [19], the gray-shaded region is excluded by neutrino trident production [27] and taken from Ref. [21]. The red crosses at $(m_{Z'}, g') = (135 \text{ MeV}, 10^{-3})$, $(219 \text{ MeV}, 1.1 \times 10^{-3})$, $(334 \text{ MeV}, 1.4 \times 10^{-3})$ indicate benchmark points adopted in our numerical study, as explained in text.

III. MUON $g-2$ AND Z'

In this and following sections, we consider the *light* Z' scenarios motivated by muon $g-2$ anomaly. In Fig. 3, we give the parameter region (the blue band) in the $(m_{Z'}, g')$ plane that accounts [20] for the discrepancy, $\Delta a_\mu = (2.9 \pm 0.9) \times 10^{-9}$ [19], taking 2σ error range. The parameter space is strongly constrained [21] by neutrino trident production, the gray-shaded exclusion region. Thus, the Z' boson of $L_\mu - L_\tau$ symmetry can explain the muon $g-2$ anomaly only if $m_{Z'} \lesssim 400 \text{ MeV}$, as given in Eq. (1). In this section, we consider the $t \rightarrow cZ'$ decay in the scenario of

$$2m_\mu < m_{Z'} \lesssim 400 \text{ MeV}, \quad [\text{Scenario (ii-a)}] \quad (27)$$

which permits the $Z' \rightarrow \mu^+\mu^-$ decay.

The Z' lifetime, $\tau_{Z'}$, estimated by summing up Eqs. (24), is also given in Fig. 3 as the black-solid contours. We see that $\tau_{Z'} \lesssim 0.1 \text{ fs}$ for the muon $g-2$ favored region above the dimuon threshold. The decay length of a light Z' with energy $E_{Z'}$ is given by

$$\gamma c\tau_{Z'} \simeq 0.4 \mu\text{m} \left[\frac{2}{N_{\text{eff}}} \right] \left[\frac{10^{-3}}{g'} \right]^2 \left[\frac{0.3 \text{ GeV}}{m_{Z'}} \right]^2 \left[\frac{E_{Z'}}{10 \text{ GeV}} \right], \quad (28)$$

where $N_{\text{eff}} \simeq 2$ for $2m_\mu \ll m_{Z'} < 2m_\tau$, and $N_{\text{eff}} \simeq 1$ for $m_{Z'} < 2m_\mu$. Thus, for $m_{Z'} \gtrsim 2m_\mu$, the Z' that is motivated by muon $(g-2)$ decays promptly after production at colliders such as LHC and B factories, with

branching ratios approximately shown in Eq. (25). For $m_{Z'} < 2m_\mu$, the lifetime can be significantly longer for extremely light Z' , but its existence is simply felt as a missing energy (with no missing mass) in collider experiments, regardless of its decay.

A. FCNC B decays

As the Z' mass range in Eq. (27) is too low to explain the P'_5 and R_K anomalies, we treat rare B meson decay data as providing constraints on the effective bsZ' coupling. By $SU(2)_L$ symmetry, this also constrains the left-handed tcZ' coupling. In the light Z' scenario, rare B meson decays provide rather strong constraints, and even the right-handed tcZ' coupling becomes significantly constrained at one-loop level. We also discuss rare kaon decay constraints on the latter.

1. $B \rightarrow K^{(*)}Z'$ formulas

The light Z' can be produced directly in $B \rightarrow K^{(*)}Z'$ decays, with $Z' \rightarrow \mu^+\mu^-/\nu\bar{\nu}$. For the bsZ' couplings of Eq. (6), the branching ratio is given by⁵

$$\mathcal{B}(\bar{B} \rightarrow \bar{K}Z') = \frac{|g_{sb}^L + g_{sb}^R|^2}{64\pi} \frac{m_B^3 \beta_{BKZ'}^3}{m_{Z'}^2 \Gamma_B} [f_+^{BK}(m_{Z'}^2)]^2, \quad (29)$$

where f_+^{BK} is the $B \rightarrow K$ form factor and

$$\beta_{XYZ} \equiv \lambda^{1/2}(1, m_Y^2/m_X^2, m_Z^2/m_X^2), \quad (30)$$

with $\lambda(x, y, z)$ defined in Eq. (17). For $B \rightarrow K^*Z'$, the branching ratio can be expressed as [40]

$$\mathcal{B}(\bar{B} \rightarrow \bar{K}^*Z') = \frac{\beta_{BK^*Z'}}{16\pi m_B \Gamma_B} (|H_0|^2 + |H_+|^2 + |H_-|^2), \quad (31)$$

where the helicity amplitudes $H_{0,\pm}$ are given by

$$\begin{aligned} H_0 &= (g_{sb}^L - g_{sb}^R) \left[-\frac{1}{2}(m_B + m_{K^*})\xi A_1(m_{Z'}^2) \right. \\ &\quad \left. + \frac{m_{K^*}m_{Z'}}{m_B + m_{K^*}}(\xi^2 - 1)A_2(m_{Z'}^2) \right], \\ H_\pm &= \frac{1}{2}(g_{sb}^L - g_{sb}^R)(m_B + m_{K^*})A_1(m_{Z'}^2) \\ &\quad \pm (g_{sb}^L + g_{sb}^R) \frac{m_{K^*}m_{Z'}}{m_B + m_{K^*}} \sqrt{\xi^2 - 1}V(m_{Z'}^2), \end{aligned} \quad (32)$$

with $\xi \equiv (m_B^2 - m_{K^*}^2 - m_{Z'}^2)/(2m_{K^*}m_{Z'})$, and A_1, A_2, V are $B \rightarrow K^*$ form factors. For the form factor numerical values, we adopt the fit formulas from light-cone sum

⁵ We imply both $B^0 \rightarrow K^0Z'$ and $B^\pm \rightarrow K^\pm Z'$. A similar convention applies to $B \rightarrow K^*Z'$.

rule calculations [41, 42]. As the Z' couples to the muon through the vector current, there is no new physics contribution to $B_s \rightarrow \mu^+ \mu^-$.

For later convenience, we provide numerical expressions of the $B^+ \rightarrow K^+ Z'$ and $B^0 \rightarrow K^{*0} Z'$ branching ratios for $m_{Z'} \lesssim 400$ MeV:

$$\begin{aligned} \mathcal{B}(B^+ \rightarrow K^+ Z') &\simeq 2.2 \times 10^{12} |g_{sb}^L + g_{sb}^R|^2 \left(\frac{300 \text{ MeV}}{m_{Z'}} \right)^2, \\ \mathcal{B}(B^0 \rightarrow K^{*0} Z') &\simeq 2.4 \times 10^{12} |g_{sb}^L - g_{sb}^R|^2 \left(\frac{300 \text{ MeV}}{m_{Z'}} \right)^2 \\ &\quad + 1.4 \times 10^{10} |g_{sb}^L + g_{sb}^R|^2. \end{aligned} \quad (33)$$

Note that the $(m_B/m_{Z'})^2$ enhancement comes from the longitudinally polarized Z' .

2. $B \rightarrow K^{(*)} \mu^+ \mu^-$ data

With $\sim 50\%$ Z' decaying into muon pairs, $B \rightarrow K^{(*)} Z'$ decays would leave footprints in the dimuon mass ($q^2 = m_{\mu\mu}^2$) spectra of $B \rightarrow K^{(*)} \mu^+ \mu^-$ decays. As the SM prediction [43] is not reliable for $q^2 < 1 \text{ GeV}^2$, one challenge for low-mass new boson search is the estimation of SM background. Instead, one could take a data-based approach [44] by searching for a narrow peak in the dimuon spectrum. With full 3.0 fb^{-1} Run 1 data, the LHCb experiment has performed [45] such a dedicated search for a new hidden-sector boson χ in $B^0 \rightarrow K^{*0} \chi$ with $\chi \rightarrow \mu^+ \mu^-$. Scanning the dimuon spectrum for $214 \text{ MeV} \leq m_{\mu\mu} \leq 4350 \text{ MeV}$ and finding no evidence for a signal, upper limits of $\mathcal{O}(10^{-9})$ on $\mathcal{B}(B^0 \rightarrow K^{*0} \chi) \mathcal{B}(\chi \rightarrow \mu^+ \mu^-)$ are set for most of the m_χ range with $\tau_\chi \leq 100 \text{ ps}$.

As the LHCb analysis [45] assumed χ to be scalar, the upper limits could be different for the Z' case due to difference in efficiency. We estimated the ratio of efficiency for vector vs scalar boson, based on information in supplemental material of Ref. [45], and confirmed that the change is rather small, varying within 0–20% in the mass range of our interest. (See Appendix A for detail.) Hence, we can apply directly the limits in Ref. [45]:

$$\mathcal{B}(B^0 \rightarrow K^{*0} \chi) \mathcal{B}(\chi \rightarrow \mu\mu) \lesssim (0.8\text{-}6.3) \times 10^{-9}, \quad (\text{LHCb}) \quad (34)$$

at 95% C.L. for $214 \text{ MeV} \leq m_\chi \leq 400 \text{ MeV}$, with $\tau_\chi \ll 1 \text{ ps}$. As the width of Z' is very small, we neglect the interference between the Z' and SM contributions.

The LHCb result greatly improves the previous limit set by Belle [46]:

$$\mathcal{B}(B^0 \rightarrow K^{*0} X) \mathcal{B}(X \rightarrow \mu\mu) \lesssim (2.3\text{-}5.0) \times 10^{-8}, \quad (\text{Belle}) \quad (35)$$

at 90% C.L. for a vector boson X with mass in $212 \text{ MeV} \leq m_X \leq 300 \text{ MeV}$. But the Belle result complements LHCb for the range $212 \text{ MeV} \leq m_X \leq 214 \text{ MeV}$ just above the dimuon threshold of 211.3 MeV .

There are no existing results for the dedicated search of low-mass new bosons in the $B \rightarrow K \mu^+ \mu^-$ mode. We stress the importance of search in this mode, as the two decay modes are complementary in probing the chiral structure of bsZ' couplings: the $B \rightarrow K Z'$ rate depends on the vector-like combination $g_{sb}^L + g_{sb}^R$, while the $B \rightarrow K^* Z'$ rate is sensitive to the axial-vector combination $g_{sb}^L - g_{sb}^R$, as can be read from Eq. (33).

In a previous study [22], published before the advent of the LHCb analysis [45], we attempted at constraining the Z' effect using existing LHCb data for $B^+ \rightarrow K^+ \mu^+ \mu^-$. We chose the 1 fb^{-1} result [47] instead of the 3 fb^{-1} one [48], as the latter provides the dimuon spectrum only for $q^2 > 0.1 \text{ GeV}^2 \simeq (316 \text{ MeV})^2$, which covers only half the Z' mass range in Scenario (ii-a). The 1 fb^{-1} result, however, gives the spectrum for $q^2 > 0.05 \text{ GeV}^2$, which can probe $m_{Z'}$ down to 224 MeV . In contrast to $B \rightarrow K^* \mu^+ \mu^-$, the photon peak is absent in $B^+ \rightarrow K^+ \mu^+ \mu^-$, and the measured q^2 spectrum [47] is rather flat in the low q^2 range, with average differential branching ratio $d\mathcal{B}/dq^2 = (2.41 \pm 0.22) \times 10^{-8} \text{ GeV}^{-2}$ in $1 \text{ GeV}^2 < q^2 < 6 \text{ GeV}^2$. Treating this as background, we subtracted it from the measured value of $d\mathcal{B}/dq^2 = (2.85 \pm 0.30) \times 10^{-8} \text{ GeV}^{-2}$ in the lowest q^2 bin of $0.05 \text{ GeV}^2 < q^2 < 2.00 \text{ GeV}^2$. We then estimated the allowed range of the Z' contribution in this bin: $\Delta\mathcal{B}(B^+ \rightarrow K^+ \mu^+ \mu^-) = (0.86 \pm 0.59) \times 10^{-8}$. At 2σ , this reads [22]

$$\mathcal{B}(B^+ \rightarrow K^+ Z') \mathcal{B}(Z' \rightarrow \mu^+ \mu^-) \lesssim 2.0 \times 10^{-8}, \quad (\text{“LHCb”}) \quad (36)$$

for $224 \text{ MeV} \lesssim m_{Z'} \lesssim 1414 \text{ MeV}$.

3. $B \rightarrow K^{(*)} \nu\bar{\nu}$ data

In Scenario (ii-a), the other $\sim 50\%$ of Z' bosons decay into neutrino pairs, resulting in $B \rightarrow K^{(*)} \nu\bar{\nu}$. Sensitivities of experimental searches for $B \rightarrow K^{(*)} \nu\bar{\nu}$ by the BaBar [49] and Belle [50] experiments are still above the SM level. For our purpose, the BaBar result [49] is useful, as model-independent constraints on BSM effects are given for spectra of $s_B \equiv m_{\nu\nu}^2/m_B^2$ bin by bin. From Fig. 6 of Ref. [49], the first bin $0 < s_B < 0.1$, or $0 < m_{\nu\nu} \lesssim 1670 \text{ MeV}$, gives the constraints $\Delta\mathcal{B}(B^+ \rightarrow K^+ \nu\bar{\nu}) = (0.35_{-0.15}^{+0.60}) \times 10^{-5}$ and $\Delta\mathcal{B}(B^+ \rightarrow K^{*+} \nu\bar{\nu}) = (-0.1_{-0.3}^{+1.9}) \times 10^{-5}$. The other two decay modes with K^0 or K^{*0} give weaker limits. The K^+ channel favors nonzero BSM effects due to the observation of a small excess over the expected background. But the probability to observe such an excess in the signal region is 8.4%, hence is not significant. The above limits at 2σ imply, for $0 < m_{Z'} \lesssim 1670 \text{ MeV}$,

$$\begin{aligned} 0.05 < 10^5 \mathcal{B}(B^+ \rightarrow K^+ Z') \mathcal{B}(Z' \rightarrow \nu\bar{\nu}) &< 1.55, \\ 10^5 \mathcal{B}(B^+ \rightarrow K^{*+} Z') \mathcal{B}(Z' \rightarrow \nu\bar{\nu}) &< 3.7. \end{aligned} \quad (\text{BaBar}) \quad (37)$$

Given the Z' branching ratios $\mathcal{B}_{\mu\mu} \sim \mathcal{B}_{\nu\nu} \sim 1/2$, the excess in $B^+ \rightarrow K^+ \nu\bar{\nu}$ is not compatible with the LHCb

limit on $B^+ \rightarrow K^+ Z' (\rightarrow \mu^+ \mu^-)$, Eq. (36). In Scenario (ii-a), we therefore treat the BaBar limits just as a reference, except when the Z' mass is close to the dimuon threshold and the $B \rightarrow K^{(*)} \mu^+ \mu^-$ limits do not apply.

B. $t \rightarrow cZ'$ via left-handed current

The $B \rightarrow K^* Z'$ rate is sensitive to the combination $g_{sb}^L - g_{sb}^R$, while its dependence on $g_{sb}^L + g_{sb}^R$ is weaker, as can be seen from Eq. (33). Hence, the limits on $B^0 \rightarrow K^{*0} Z' (\rightarrow \mu^+ \mu^-)$ by LHCb, Eq. (34), draw an ellipse extending along the $g_{sb}^L = g_{sb}^R$ direction on the (g_{sb}^L, g_{sb}^R) plane for each $m_{Z'}$ value. The resulting constraints on the bsZ' couplings are $|g_{sb}^L|, |g_{sb}^R| \lesssim (2-7) \times 10^{-10}$ for $214 \text{ MeV} \leq m_{Z'} \leq 400 \text{ MeV}$.

The constraints on the bsZ' couplings are improved if the limit on $B^+ \rightarrow K^+ Z' (\rightarrow \mu^+ \mu^-)$ extracted from the LHCb data, Eq. (36), is further imposed: $|g_{sb}^L|, |g_{sb}^R| \lesssim 1 \times 10^{-10}$ for $224 \text{ MeV} \lesssim m_{Z'} \leq 400 \text{ MeV}$, which is rather stable w.r.t. $m_{Z'}$. The limit implies

$$m_Q \gtrsim 670 \text{ TeV} \sqrt{|Y_{Qs}^* Y_{Qb}| \left(\frac{m_{Z'}}{300 \text{ MeV}} \right) \left(\frac{10^{-3}}{g'} \right)}, \quad (38)$$

which is an order of magnitude larger than in Scenario (i) [Eq. (11)]. Assuming the $SU(2)_L$ relation $g_{ct}^L \simeq g_{sb}^L$, then, we obtain bounds on the left-handed current contribution to the $t \rightarrow cZ'$ branching ratio:

$$\mathcal{B}(t \rightarrow cZ')_{\text{LH}} \lesssim (3-4) \times 10^{-15}, \quad (39)$$

for $224 \text{ MeV} \lesssim m_{Z'} \leq 400 \text{ MeV}$. These values would be too small to measure even with the high-luminosity LHC upgrade. [See Eq. (26) for a naive expectation.]

For $214 \text{ MeV} \leq m_{Z'} \lesssim 224 \text{ MeV}$, the $B^+ \rightarrow K^+ Z' (\rightarrow \mu^+ \mu^-)$ limit does not apply, and bounds on the $t \rightarrow cZ'$ rate are weakened:

$$\mathcal{B}(t \rightarrow cZ')_{\text{LH}} \lesssim (2-4) \times 10^{-13}, \quad (40)$$

for $214 \text{ MeV} \leq m_{Z'} \lesssim 224 \text{ MeV}$. In the narrow interval $212 \text{ MeV} \leq m_{Z'} < 214 \text{ MeV}$, the LHCb limits on $B^0 \rightarrow K^{*0} Z' (\rightarrow \mu^+ \mu^-)$ are taken over by the Belle limits, Eq. (35), which give an order of magnitude weaker bounds on $\mathcal{B}(t \rightarrow cZ')_{\text{LH}}$ than the case for $214 \text{ MeV} \leq m_{Z'} \lesssim 224 \text{ MeV}$. The remaining spot of $211.3 \text{ MeV} \lesssim m_{Z'} < 212 \text{ MeV}$, just above the dimuon threshold, is still constrained by the BaBar limits on $B \rightarrow K^{(*)} \nu \bar{\nu}$, Eq. (37), leading to $\mathcal{B}(t \rightarrow cZ')_{\text{LH}} \lesssim 4 \times 10^{-12}$, which is further diluted by a small Z' branching ratio $\mathcal{B}(Z' \rightarrow \mu^+ \mu^-) \lesssim 10\%$. Note that the excess in $B^+ \rightarrow K^+ \nu \bar{\nu}$ does not necessarily imply a nonzero $g_{sb}^L \simeq g_{ct}^L$, as g_{sb}^R alone can still explain the excess. These values of $\mathcal{B}(t \rightarrow cZ')_{\text{LH}}$ would be still too small for measurements at the LHC.

In deriving the limits on the left-handed current contribution to $\mathcal{B}(t \rightarrow cZ')$, we assumed the $SU(2)_L$ relation $g_{ct}^L \simeq g_{sb}^L$. This is valid for $Y_{Qt} \sim Y_{Qc}$, but does not hold

in general. More precisely, the $SU(2)_L$ relation is given by Eq. (5): $Y_{Qb} = V_{cb} Y_{Qc} + V_{tb} Y_{Qt} \simeq A \lambda^2 Y_{Qc} + Y_{Qt}$, and $Y_{Qs} = V_{cs} Y_{Qc} + V_{ts} Y_{Qt} \simeq Y_{Qc} - A \lambda^2 Y_{Qt}$, where $A \simeq 0.81$ [1], and Y_{Qu} is taken to be zero to avoid D meson constraints. A remarkable deviation from our assumption occurs when $Y_{Qc}/Y_{Qt} \sim \lambda^2$: Y_{Qs} vanishes for $Y_{Qc} \simeq A \lambda^2 Y_{Qt}$, hence, $g_{sb}^L \propto Y_{Qs}^* Y_{Qb} \simeq 0$ (and $g_{ds}^L \simeq 0$). This allows a large g_{ct}^L without violating the $b \rightarrow sZ'$ (and $s \rightarrow dZ'$) constraints. Yet, this implies $Y_{Qd} \sim \lambda Y_{Qc}$ with $Y_{Qb} \simeq Y_{Qt}$, hence, $g_{db}^L \propto Y_{Qd}^* Y_{Qb} \sim \lambda g_{ct}^L$, which would be constrained by the measurement of the $B^+ \rightarrow \pi^+ \mu^+ \mu^-$ decay by LHCb [51, 52], as well as B - \bar{B} mixing. We do not pursue such an extreme case in this paper.

Before moving on, we briefly mention the B_s meson mixing constraint. For light Z' , the local $(\bar{s}b)(\bar{s}b)$ box operator construction in usual renormalization group analysis is not valid, as the Z' remains a dynamical degree of freedom at the m_B scale. Here, we simply recover the momentum dependence in the Z' propagator in the usual heavy Z' formula and set the Z' momentum to the B_s mass scale. To see the impact of this constraint, for simplicity, we only include the left-handed bsZ' coupling effects. Employing the unitarity gauge and the vacuum insertion approximation [40], we find that the B_s - \bar{B}_s mixing amplitude is modified as

$$\begin{aligned} \frac{M_{12}}{M_{12}^{\text{SM}}} &\simeq 1 - \frac{(g_{sb}^L)^2 v^2}{m_{B_s}^2 - m_{Z'}^2} \left(1 - \frac{5 m_{B_s}^2}{8 m_{Z'}^2} \right) \\ &\times \left[\frac{g_2^2}{16\pi^2} (V_{ts}^* V_{tb})^2 S_0 \right]^{-1}. \end{aligned} \quad (41)$$

Allowing 15% BSM effect, we obtain $|g_{sb}^L| \lesssim 2 \times 10^{-6} (m_{Z'}/300 \text{ MeV})$, four orders of magnitude weaker than the constraint from $B \rightarrow K^{(*)} Z' (\rightarrow \mu^+ \mu^-)$.

C. Right-handed tcZ' coupling: loop-induced down-quark sector FCNCs

The right-handed tcZ' coupling induces FCNCs in down-type quark sector at one-loop level. More precisely, the $SU(2)_L$ singlet vector-like quark U , responsible for the effective right-handed tcZ' coupling, mediates the diagram in Fig. 4, leading to extra contributions to effective sdZ' and bsZ' couplings. Assisted by the SM charged current couplings of the W boson to left-handed quarks, not only tcZ' , but also flavor-diagonal ttZ' and ccZ' contribute. These contributions are loop, chirality and CKM suppressed. There are thus no significant impacts for the heavy Z' . However, for light Z' , the loop-induced FCNC decays give meaningful constraints, as the meson decay rates are hugely enhanced due to on-shell nature of the Z' , compensating these suppressions.

In estimating the loop-induced FCNC couplings, for simplicity, we set $Y_{Qd_i} = Y_{Dd_i} = 0$ ($i = 1, 2, 3$) to turn off the tree-level FCNC couplings in the down-type quark sector. We further set $Y_{Uu} = 0$ to avoid constraints from

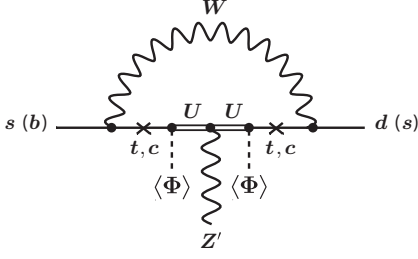


FIG. 4. Feynman diagram that induces the effective sdZ' (bsZ') coupling at one-loop through Yukawa couplings Y_{Ut} and Y_{Uc} . The crosses indicate quark mass insertions which flip chirality for t or c . We included similar contribution from the would-be Nambu-Goldstone bosons.

D meson decays and mixing, for sake of maximizing the $t \rightarrow cZ'$ decay rate. We are then left with the Yukawa mixing couplings for the vector-like quark U to right-handed top or charm quarks, Y_{Ut} and Y_{Uc} .

Working in the 't Hooft-Feynman gauge, we calculate the diagram of Fig. 4, as well as similar contributions with the would-be Nambu-Goldstone bosons. We neglect the external momenta as usual, but keep all internal momenta, including the one for the vector-like quark U . We then obtain the loop-induced effective couplings [22]:

$$\mathcal{L}_{\text{eff}} \supset \Delta g_{d_i d_j}^L \bar{d}_i \gamma^\alpha d_j L Z'_\alpha + \text{h.c.}, \quad (42)$$

where $i, j = 1, 2, 3$, and

$$\Delta g_{d_i d_j}^L = \frac{g' v_\Phi^2}{32\pi^2 v^2} [V_{td_j} V_{td_i}^* \kappa_{tt} f_{tt} + (V_{td_j} V_{cd_i}^* \kappa_{tc} + V_{cd_j} V_{td_i}^* \kappa_{ct}) f_{ct} + V_{cd_j} V_{cd_i}^* \kappa_{cc} f_{cc}], \quad (43)$$

with

$$\kappa_{u_k u_l} = Y_{U u_k} Y_{U u_l}^* \frac{m_{u_k} m_{u_l}}{m_U^2}, \quad (44)$$

and

$$\begin{aligned} f_{tt} &\simeq \frac{3m_W^2}{m_t^2 - m_W^2} \left(1 - \frac{m_W^2}{m_t^2 - m_W^2} \log \frac{m_t^2}{m_W^2} \right) + \log \frac{m_U^2}{m_t^2}, \\ f_{ct} &\simeq 1 + \log \frac{m_U^2}{m_t^2} + \frac{3m_W^2}{m_t^2 - m_W^2} \log \frac{m_t^2}{m_W^2}, \\ f_{cc} &\simeq 4 \log \frac{m_W^2}{m_c^2} + \log \frac{m_U^2}{m_W^2} - 3. \end{aligned} \quad (45)$$

The expressions for these loop functions are in the large m_U limit. Exact expressions used in our numerical study are given in Appendix B.

In the loop-induced bsZ' and bdZ' couplings, Eq. (43), the top-top loop contribution dominates due to chiral factor, so long as Y_{Uc}/Y_{Ut} is not too large. Then, $\Delta g_{db}^L/\Delta g_{sb}^L \simeq V_{td}^*/V_{ts}^* \sim \lambda$, hence, the ratio $\mathcal{B}(b \rightarrow dZ')/\mathcal{B}(b \rightarrow sZ') \sim \lambda^2 \simeq 0.05$ is SM-like. For large Y_{Uc} (e.g. $Y_{Uc}/Y_{Ut} \gtrsim 4$ for $m_U = 2$ TeV), the top-charm loop contribution becomes dominant. Even in

this case, $\Delta g_{db}^L/\Delta g_{sb}^L \simeq V_{cd}^*/V_{cs}^* \sim \lambda$, hence, the ratio $\mathcal{B}(b \rightarrow dZ')/\mathcal{B}(b \rightarrow sZ')$ is still SM-like. Thus, the better measured $b \rightarrow s$ decays are more suitable to watch Z' effect than $b \rightarrow d$. We consider $b \rightarrow sZ'$ and $s \rightarrow dZ'$ decays below.

D. FCNC K decays

1. $K \rightarrow \pi Z'$ formulas

One can obtain $\mathcal{B}(B \rightarrow K^{(*)} Z')$ for loop-induced bsZ' coupling by replacing $g_{sb}^L \rightarrow \Delta g_{sb}^L$, $g_{sb}^R \rightarrow 0$ in Eqs. (29) and (31). Then, $\mathcal{B}(B \rightarrow K^{(*)} Z') \simeq \mathcal{B}(B \rightarrow K Z')$, as can be seen from Eq. (33). Hence, the LHCb limits on $B^0 \rightarrow K^{*0} \chi(\rightarrow \mu^+ \mu^-)$, Eq. (34), give the strongest constraint in most $m_{Z'}$ ranges of Scenario (ii-a).

The loop-induced sdZ' coupling causes $K \rightarrow \pi Z'$ for $m_{Z'} < m_K - m_\pi$, leading to $K \rightarrow \pi \mu^+ \mu^-$ and $K \rightarrow \pi \nu \bar{\nu}$ decays. The branching ratios for $K^+ \rightarrow \pi^+ Z'$ and $K_L \rightarrow \pi^0 Z'$ decays are given by

$$\begin{aligned} \mathcal{B}(K^+ \rightarrow \pi^+ Z') &= \frac{|\Delta g_{ds}^L|^2}{64\pi} \frac{m_{K^+}^3}{m_{Z'}^2 \Gamma_{K^+}} \beta_{K^+ \pi^+ Z'}^3 \left[f_+^{K^+ \pi^+}(m_{Z'}) \right]^2, \\ \mathcal{B}(K_L \rightarrow \pi^0 Z') &= \frac{[\text{Im}(\Delta g_{ds}^L)]^2}{64\pi} \frac{m_{K_L}^3}{m_{Z'}^2 \Gamma_{K_L}} \beta_{K_L \pi^0 Z'}^3 \left[f_+^{K^0 \pi^0}(m_{Z'}) \right]^2, \end{aligned} \quad (46)$$

where $\beta_{K\pi Z'}$ is defined by Eq. (30), and $f_+^{K\pi}$ are the $K \rightarrow \pi$ form factors. For the latter, we adopt the result of Ref. [53], which is based on the partial NNLO calculation with isospin-breaking effects in chiral perturbation theory. In estimating the $K_L \rightarrow \pi^0 Z'$ rate, we took $|K_L\rangle \simeq (|K^0\rangle + |\bar{K}^0\rangle)/\sqrt{2}$ with the phase convention where $CP|K^0\rangle = -|\bar{K}^0\rangle$, neglecting CP violation in kaon mixing. The branching ratio for $K_S \rightarrow \pi^0 Z'$ can be obtained from the one for $K_L \rightarrow \pi^0 Z'$ with the replacements: $\text{Im}(\Delta g_{ds}^L) \rightarrow \text{Re}(\Delta g_{ds}^L)$ and $\tau_{K_L} \rightarrow \tau_{K_S}$.

2. $K \rightarrow \pi \mu^+ \mu^-$ data

In SM, the $K^+ \rightarrow \pi^+ \mu^+ \mu^-$ decay is dominated by long-distance effects via one-photon exchange $K^+ \rightarrow \pi^+ \gamma^*$. The decay can be described by chiral perturbation theory [55] with the dimuon invariant mass spectrum $d\Gamma/dz \propto |W(z)|^2$, where $z \equiv m_{\mu\mu}^2/m_{K^+}^2$ and $W(z)$ is the $K \rightarrow \pi \gamma^*$ form factor. The most precise value for $\mathcal{B}(K^+ \rightarrow \pi^+ \mu^+ \mu^-)$ by a single measurement comes from the NA48/2 experiment [54] at the CERN SPS. The measured z -spectrum in the whole kinematic range of $4m_\mu^2/m_{K^+}^2 \leq z \leq (1 - m_{\pi^+}/m_{K^+})^2$, corresponding to $211 \text{ MeV} \lesssim m_{\mu\mu} \lesssim 354 \text{ MeV}$, is reasonably described by various form factor models. In particular, the measured z -spectrum does not exhibit significant excesses over the

fit curve by the linear form factor model. Here, we attempt a simple data-based approach to extract reasonable sizes for possible Z' effects.

In a previous study [22], we focused on the largest upward deviation from the fit curve in the z -spectrum of NA48/2, which is located in the $z \in (0.32, 0.34)$ bin, corresponding to $m_{\mu\mu} \in (279, 288)$ MeV. Subtracting the fit value from the measured one, we read the allowed range for an extra contribution: $\Delta(d\Gamma/dz) \simeq (2.5 \pm 1.5) \times 10^{-24}$ GeV. This corresponds to the deviation of the branching ratio in $m_{\mu\mu} \in (279, 288)$ MeV: $\Delta\mathcal{B}(K^+ \rightarrow \pi^+\mu^+\mu^-) \simeq (9.4 \pm 5.6) \times 10^{-10}$. Allowing 2σ range, we estimate the limit on the Z' contribution: $\mathcal{B}(K^+ \rightarrow \pi^+Z')\mathcal{B}(Z' \rightarrow \mu^+\mu^-) \lesssim 2.1 \times 10^{-9}$ for 279 MeV $\lesssim m_{Z'} \lesssim 288$ MeV. The constraint is tighter for other Z' mass values in 211 MeV $\lesssim m_{\mu\mu} \lesssim 354$ MeV. For instance, we obtain

$$\mathcal{B}(K^+ \rightarrow \pi^+Z')\mathcal{B}(Z' \rightarrow \mu\mu) \lesssim 1.1 \times 10^{-9} \text{ ("NA48/2")} \quad (47)$$

for $327 \text{ MeV} < m_{Z'} \lesssim 335 \text{ MeV}$, and

$$\mathcal{B}(K^+ \rightarrow \pi^+Z')\mathcal{B}(Z' \rightarrow \mu\mu) \lesssim 1.2 \times 10^{-9} \text{ ("NA48/2")} \quad (48)$$

for $2m_\mu < m_{Z'} \lesssim 221 \text{ MeV}$.

For $K_L \rightarrow \pi^0\mu^+\mu^-$, the current best limit comes from KTeV [56] at Fermilab, giving the 90% C.L. limit

$$\mathcal{B}(K_L \rightarrow \pi^0\mu^+\mu^-) < 3.8 \times 10^{-10}. \text{ (KTeV)} \quad (49)$$

This is above the SM prediction of $(1.29_{-0.23}^{+0.24}) \times 10^{-11}$ [57]. We thus impose the above limit on $\mathcal{B}(K_L \rightarrow \pi^0Z')\mathcal{B}(Z' \rightarrow \mu^+\mu^-)$ for $2m_\mu < m_{Z'} < 350$ MeV, covered by the kinematic selection of the KTeV analysis.

The $K_S \rightarrow \pi^0\mu^+\mu^-$ mode was measured by NA48/1 [58] at CERN SPS, giving $\mathcal{B}(K_S \rightarrow \pi^0\mu^+\mu^-) = [2.9_{-1.2}^{+1.5}(\text{stat}) \pm 0.2(\text{syst})] \times 10^{-9}$. This was used as input in the SM prediction of $K_L \rightarrow \pi^0\mu^+\mu^-$ [57] to control the indirect CP violating contribution. For the possible Z' contribution, isospin symmetry implies $\mathcal{B}(K_S \rightarrow \pi^0Z') \lesssim (\tau_{K_S}/\tau_{K^+})\mathcal{B}(K^+ \rightarrow \pi^0Z') \simeq 0.007 \times \mathcal{B}(K^+ \rightarrow \pi^0Z')$. Given that the experimental sensitivity on the $K^+ \rightarrow \pi^+Z'(\rightarrow \mu^+\mu^-)$ branching ratio is around 10^{-9} , the above isospin relation constrains the $K_S \rightarrow \pi^0Z'(\rightarrow \mu^+\mu^-)$ branching ratio to be within $\sim 10^{-11}$, which may be beyond the sensitivity of NA48/1 data.

3. $K \rightarrow \pi\nu\bar{\nu}$ data

For $K^+ \rightarrow \pi^+\nu\bar{\nu}$ decay, the E949 experiment [59] at BNL, together with its predecessor E787, reported $\mathcal{B}(K^+ \rightarrow \pi^+\nu\bar{\nu}) = (1.73_{-1.05}^{+1.15}) \times 10^{-10}$, which is consistent with SM prediction of $(8.25 \pm 0.64) \times 10^{-11}$ [57]. The measurement error is large and E787/E949 [60] also reported the 90% C.L. upper limit of $\mathcal{B}(K^+ \rightarrow \pi^+\nu\bar{\nu}) <$

3.35×10^{-10} . We remark, however, that the experimental analyses utilized limited intervals for the pion momentum p_{π^+} , or equivalently the neutrino pair mass $m_{\nu\nu}$, to avoid blinding backgrounds from $K^+ \rightarrow \pi^+\pi^0$ and $K^+ \rightarrow \pi^+\pi^-\pi^+/\pi^+\pi^0\pi^0$: one is the $\pi\nu\bar{\nu}(1)$ region, where $211 \text{ MeV} < p_{\pi^+} < 229 \text{ MeV}$, or $0 \leq m_{\nu\nu} \lesssim 116$ MeV; the other is the $\pi\nu\bar{\nu}(2)$ region, where $140 \text{ MeV} < p_{\pi^+} < 199 \text{ MeV}$, or $152 \text{ MeV} \lesssim m_{\nu\nu} \lesssim 261 \text{ MeV}$. The kinematic selection of the $K^+ \rightarrow \pi^+\nu\bar{\nu}$ experiments has an interesting implication for $K_L \rightarrow \pi^0\nu\bar{\nu}$ search [22], as we will discuss in the next section.

The E787/E949 data have been used also for a dedicated search [60] of a two-body decay $K^+ \rightarrow \pi^+P^0$ with $P^0 \rightarrow \nu\bar{\nu}$, where P^0 is a hypothetical short-lived particle. The upper limits on $\mathcal{B}(K^+ \rightarrow \pi^+P^0)\mathcal{B}(P^0 \rightarrow \nu\bar{\nu})$ were given for the mass ranges of $0 \leq m_{P^0} \lesssim 125$ MeV or $150 \text{ MeV} \lesssim m_{P^0} \lesssim 260$ MeV, which correspond to $\pi\nu\bar{\nu}(1)$ or $\pi\nu\bar{\nu}(2)$ regions, respectively. In the mass range which is relevant to Scenario (ii-a), the 90% C.L. upper limits increases almost monotonically with mass within

$$\mathcal{B}(K^+ \rightarrow \pi^+P^0)\mathcal{B}(P^0 \rightarrow \nu\bar{\nu}) \lesssim (0.4\text{-}5) \times 10^{-9}, \text{ (E949)} \quad (50)$$

for $2m_\mu < m_{P^0} \lesssim 260$ MeV.

To facilitate the discussion in Scenario (ii-b), we also quote 90% C.L. upper limits for typical P^0 masses below the dimuon threshold by setting $\mathcal{B}(P^0 \rightarrow \nu\bar{\nu}) = 1$. For $0 \leq m_{P^0} \lesssim 125$ MeV, the strongest (weakest) bound is attained for $m_{P^0} \simeq 95$ (125) MeV with $\mathcal{B}(K^+ \rightarrow \pi^+P^0) \lesssim 5 \times 10^{-11}$ (4×10^{-9}). The bound is rather stable for $0 \leq m_{P^0} \lesssim 40$ MeV with $\mathcal{B}(K^+ \rightarrow \pi^+P^0) \lesssim 10^{-10}$. For $150 \text{ MeV} \lesssim m_{P^0} < 2m_\mu$, the strongest (weakest) bound is attained for $m_{P^0} \simeq 190$ (150) MeV with $\mathcal{B}(K^+ \rightarrow \pi^+P^0) \lesssim 4 \times 10^{-10}$ (10^{-8}).

For the pocket $125 \text{ MeV} \lesssim m_{Z'} \lesssim 150$ MeV around π^0 mass, the upper limit can be still obtained by using the $\pi^0 \rightarrow \nu\bar{\nu}$ search in $K^+ \rightarrow \pi^+\pi^0$ by E949 [61]: $\mathcal{B}(\pi^0 \rightarrow \nu\bar{\nu}) < 2.7 \times 10^{-7}$ at 90% C.L. In this search, charged pions with momentum in $198 \text{ MeV} < p_{\pi^+} < 212 \text{ MeV}$ were selected, corresponding to $112 \text{ MeV} \lesssim m_{\nu\nu} \lesssim 155 \text{ MeV}$, hence the π^0 -pocket can be fully covered. Combining with $\mathcal{B}(K^+ \rightarrow \pi^+\pi^0) \simeq 20.7\%$ [1], one has

$$\mathcal{B}(K^+ \rightarrow \pi^+Z') < 5.6 \times 10^{-8}, \text{ (E949)} \quad (51)$$

at 90% C.L. for $112 \lesssim m_{Z'} \lesssim 155$ MeV.

The $K_L \rightarrow \pi^0\nu\bar{\nu}$ decay has been searched for by the E391a experiment [62] at the KEK proton synchrotron, setting the 90% C.L. upper limit

$$\mathcal{B}(K_L \rightarrow \pi^0\nu\bar{\nu}) < 2.6 \times 10^{-8}, \text{ (E391a)} \quad (52)$$

without any particular cut on $m_{\nu\nu}$. This is far above the SM prediction of $(2.60 \pm 0.37) \times 10^{-11}$ [57]. Therefore, we impose Eq. (52) on $\mathcal{B}(K_L \rightarrow \pi^0Z')\mathcal{B}(Z' \rightarrow \nu\bar{\nu})$ for $m_{Z'} < m_{K_L} - m_{\pi^0} \simeq 363$ MeV. Note that in Scenario (ii-a), where $m_{Z'} > 2m_\mu$, the KTeV limit, Eq. (49), gives stronger constraint in general, as $\mathcal{B}_{\mu\mu} \sim \mathcal{B}_{\nu\nu} \sim 1/2$.

Mode	Experiment	$m_{Z'} = 334$ MeV	$m_{Z'} = 219$ MeV	$m_{Z'} = 135$ MeV	Comment
$B^0 \rightarrow K^{*0} Z' (\rightarrow \mu^+ \mu^-)$	LHCb [45]	$< 4.41 \times 10^{-9}$	$< 6.29 \times 10^{-9}$	–	See Eq. (53).
$B^+ \rightarrow K^+ Z' (\rightarrow \nu \bar{\nu})$	BaBar [49]	$(0.05, 1.55) \times 10^{-5}$	$(0.05, 1.55) \times 10^{-5}$	$(0.05, 1.55) \times 10^{-5}$	See Eq. (37).
$K^+ \rightarrow \pi^+ Z' (\rightarrow \mu^+ \mu^-)$	“NA48/2” [54]	$\lesssim 1.1 \times 10^{-9}$	$\lesssim 1.2 \times 10^{-9}$	–	See Eqs. (47), (48).
$K_L \rightarrow \pi^0 Z' (\rightarrow \mu^+ \mu^-)$	KTeV [56]	$< 3.8 \times 10^{-10}$	$< 3.8 \times 10^{-10}$	–	See Eq. (49).
$K^+ \rightarrow \pi^+ Z' (\rightarrow \nu \bar{\nu})$	E787/E949 [60, 61]	–	$\lesssim 5 \times 10^{-10}$	$< 5.6 \times 10^{-8}$	See Eqs. (50), (51).
$K_L \rightarrow \pi^0 Z' (\rightarrow \nu \bar{\nu})$	E391a [62]	$< 2.6 \times 10^{-8}$	$< 2.6 \times 10^{-8}$	$< 2.6 \times 10^{-8}$	See Eq. (52).

TABLE I. Summary of B and K decay constraints for the three benchmark points in scenarios (ii-a) and (ii-b): $m_{Z'} = 334, 219, 135$ MeV. The numbers shown in third to fifth column are the allowed ranges for each branching ratios, used in Figs. 5–8. See text, and in particular the referred equations (last column), for detail.

There are no existing constraints on $K_S \rightarrow \pi^0 \nu \bar{\nu}$, where the branching ratio is suppressed by $\tau_{K_S}/\tau_{K_L} \ll 1$ compared to $K_L \rightarrow \pi^0 \nu \bar{\nu}$.

E. $t \rightarrow cZ'$ via right-handed current

We can now combine all B and K decay data to constrain the right-handed current contribution $\mathcal{B}(t \rightarrow cZ')_{\text{RH}}$. For illustration, we take the two benchmark points (shown by red crosses in Fig. 3):

- $m_{Z'} = 334$ MeV, $g' = 1.4 \times 10^{-3}$, $m_U = 2$ TeV,
- $m_{Z'} = 219$ MeV, $g' = 1.1 \times 10^{-3}$, $m_U = 2$ TeV.

The Z' mass values are chosen such that the LHCb limit for $B^0 \rightarrow K^{*0} \chi (\rightarrow \mu^+ \mu^-)$, Eq. (34), is weakened to be tolerant for a possible large $t \rightarrow cZ'$ rate: $m_{Z'} = 219$ MeV is one of the points which give the weakest limit in the *whole* range of $214 \text{ MeV} \leq m_{Z'} \leq 400 \text{ MeV}$, while $m_{Z'} = 334$ MeV gives the weakest limit in the *high* mass region $260 \text{ MeV} \lesssim m_{Z'} \leq 400 \text{ MeV}$, where the E949 limits for $K^+ \rightarrow \pi^+ P^0 (\rightarrow \nu \bar{\nu})$ do not apply. The two benchmark points are phenomenological representatives of B and K decay constraints. The 95% C.L. upper limits by LHCb [45] are ⁶

$$\mathcal{B}(B^0 \rightarrow K^{*0} \chi) \mathcal{B}(\chi \rightarrow \mu^+ \mu^-) < \begin{cases} 4.41 \times 10^{-9} & (m_\chi = 334 \text{ MeV}), \\ 6.29 \times 10^{-9} & (m_\chi = 219 \text{ MeV}). \end{cases} \quad (53)$$

We neglect again the changes in efficiencies from scalar boson case. For loop-induced bsZ' coupling, where $g_{sb}^R = 0$, the changes are indeed extremely small, up to 6% in the mass range of our interest (See Appendix A). The B and K constraints are summarized in Table I.

In Fig. 5 [left], we give contours of $\mathcal{B}(t \rightarrow cZ')_{\text{RH}}$ as black-solid lines in the (Y_{U_t}, Y_{U_c}) plane for $m_{Z'} = 334$

MeV benchmark point. The meson decay constraints are imposed by taking into account the Z' branching ratios: $\mathcal{B}_{\mu\mu} \simeq 48\%$, $\mathcal{B}_{\nu\nu} \simeq 52\%$. The pink-shaded region is allowed by the LHCb bound on $B^0 \rightarrow K^{*0} \chi (\rightarrow \mu^+ \mu^-)$ in Eq. (53). The light-green-shaded regions are favored by the mild excess in BaBar data for $B^+ \rightarrow K^+ \nu \bar{\nu}$ at 2σ [Eq. (37)]. The semi-transparent dark-gray shaded region represents 2σ exclusion by the NA48/2 data for $K^+ \rightarrow \pi^+ \mu^+ \mu^-$, Eq. (47), from our illustration of the limit on the Z' effect. The purple-solid lines are 90% C.L. exclusion by KTeV data for $K_L \rightarrow \pi^0 \mu^+ \mu^-$, Eq. (49).

All the data have better sensitivity for Y_{U_t} than Y_{U_c} , as the top-top loop contribution dominates the loop-induced effective couplings, Eq. (43), due to m_t/m_c chiral enhancement. The LHCb limit for $B^0 \rightarrow K^{*0} \chi (\rightarrow \mu^+ \mu^-)$ provides the strongest constraint, excluding the BaBar region that could account for the $B^+ \rightarrow K^+ \nu \bar{\nu}$ excess. Nevertheless, the LHCb limit accommodates $\mathcal{B}(t \rightarrow cZ')_{\text{RH}} \gtrsim 10^{-6}$ along the funnel regions, extending towards large Y_{U_c} . However, the NA48/2 limit for $K^+ \rightarrow \pi^+ \mu^+ \mu^-$ eventually cuts down these funnels. We obtain $\mathcal{B}(t \rightarrow cZ')_{\text{RH}} \lesssim 2 \times 10^{-5}$.

We remark that $m_{Z'} = 334$ MeV is close to the kinematical limit $m_{K^+} - m_{\pi^+} \simeq 354$ MeV of $K^+ \rightarrow \pi^+ Z'$, and the NA48/2 data is less constraining than generic cases. This can be seen from the *velocity* factor in Eq. (46): $\beta_{K^+\pi^+Z'} \simeq 0.26$ for $m_{Z'} = 334$ MeV, leading to the suppression of $\mathcal{B}(K^+ \rightarrow \pi^+ Z')$ by $\beta_{K^+\pi^+Z'}^3 \simeq 0.018$, compared with, e.g. $\beta_{K^+\pi^+Z'}^3 \simeq 0.31$ (0.080) for $m_{Z'} = 219$ (300) MeV.

For $m_{Z'} > m_{K^+} - m_{\pi^+}$, the two-body decay $K^+ \rightarrow \pi^+ Z'$ is kinematically forbidden, and the NA48/2 data loses constraining power, hence $\mathcal{B}(t \rightarrow cZ')_{\text{RH}}$ can be arbitrary large along the funnels. However, the funnels imply some degree of fine-tuning between Y_{U_t} and Y_{U_c} with cancelled contributions to $b \rightarrow sZ'$. Furthermore, Y_{U_c} should not be too large to maintain perturbativity.

A similar plot for the $m_{Z'} = 219$ MeV benchmark point is given in Fig. 5 [right], where $\mathcal{B}_{\mu\mu} \simeq 28\%$, $\mathcal{B}_{\nu\nu} \simeq 72\%$. In this case, the E949 limit for $K^+ \rightarrow \pi^+ P^0 (\rightarrow \nu \bar{\nu})$ enters: $\mathcal{B}(K^+ \rightarrow \pi^+ P^0) \mathcal{B}(P^0 \rightarrow \nu \bar{\nu}) \lesssim 5 \times 10^{-10}$ at 90% C.L. [60], shown as semi-transparent dark-gray shaded exclusion region. This surpasses the NA48/2 limit for $K^+ \rightarrow \pi^+ \mu^+ \mu^-$, Eq. (48), shown by the light-gray solid

⁶ We thank M. Williams for providing us the precise upper values used in our study.

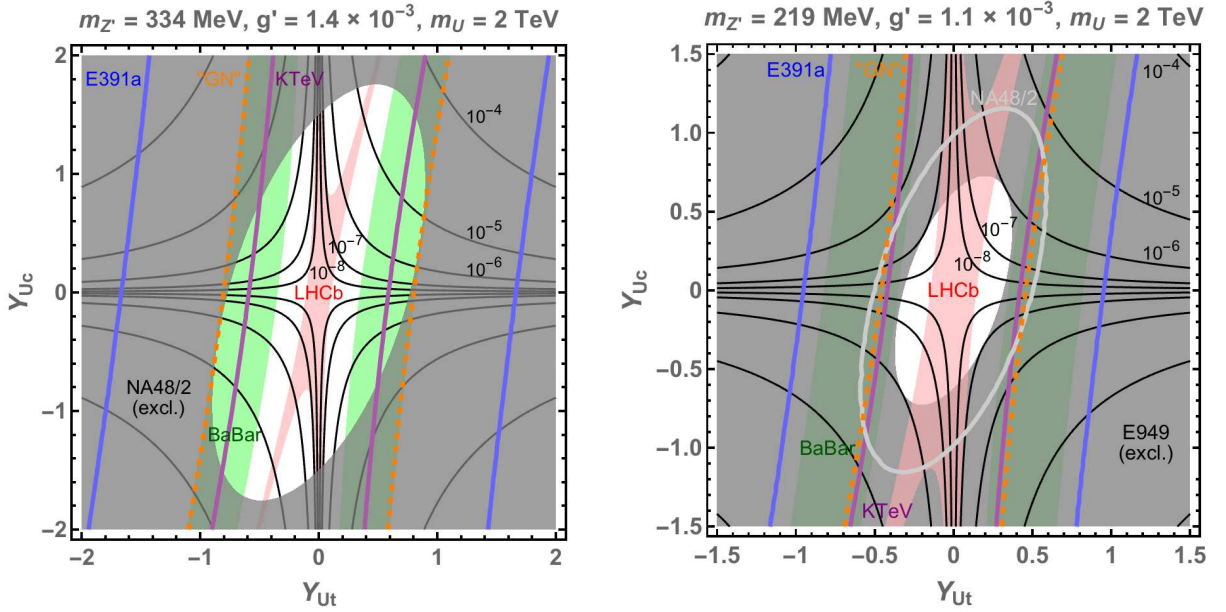


FIG. 5. [Left] Contours of $\mathcal{B}(t \rightarrow cZ')_{\text{RH}}$ are given as black-solid lines in the (Y_{Ut}, Y_{Uc}) plane for $m_{Z'} = 334$ MeV, $g' = 1.4 \times 10^{-3}$ and $m_U = 2$ TeV. The pink shaded region is allowed by the LHCb 95% C.L. limit for $B^0 \rightarrow K^{*0} \chi (\rightarrow \mu^+ \mu^-)$ in Eq. (53). The light-green shaded regions are favored by the mild excess in BaBar data for $B^+ \rightarrow K^+ \nu \bar{\nu}$ at 2σ [Eq. (37)]. The semi-transparent dark-gray shaded region represents 2σ exclusion by NA48/2 for $K^+ \rightarrow \pi^+ \mu^+ \mu^-$, Eq. (47). The purple-solid lines are 90% C.L. exclusion by KTeV for $K_L \rightarrow \pi^0 \mu^+ \mu^-$, Eq. (49). The blue-solid lines are 90% C.L. exclusion by E391a for $K_L \rightarrow \pi^0 \nu \bar{\nu}$, Eq. (52). The orange-dashed lines are the usual “GN bound” of Eq. (60), explained later. [Right] Same as left panel, but for $m_{Z'} = 219$ MeV, $g' = 1.1 \times 10^{-3}$ and $m_U = 2$ TeV. Here, the NA48/2 exclusion, Eq. (48), is shown by the light-gray solid line, while the semi-transparent dark-gray-shaded region is excluded by the E949 90% C.L. limit $\mathcal{B}(K^+ \rightarrow \pi^+ P^0) \mathcal{B}(P^0 \rightarrow \nu \bar{\nu}) \lesssim 5 \times 10^{-10}$.

ellipse in the figure. The E949 limit fully excludes the funnel regions, and we obtain $\mathcal{B}(t \rightarrow cZ')_{\text{RH}} \lesssim 0.8 \times 10^{-6}$.

The E949 limit gets stronger towards $m_{Z'} = 2m_\mu$ and generically excludes the funnel regions for $2m_\mu < m_{Z'} \lesssim 230$ MeV, leading to $\mathcal{B}(t \rightarrow cZ')_{\text{RH}} \lesssim 10^{-6}$. Remarkably, this limit on $\mathcal{B}(t \rightarrow cZ')_{\text{RH}}$ holds even in the pocket 211.3 MeV $\lesssim m_{Z'} < 212$ MeV, where neither LHCb nor Belle limits for $B^0 \rightarrow K^{*0} Z' (\rightarrow \mu^+ \mu^-)$ apply.

We have used $m_U = 2$ TeV, but obtained similar results for other m_U values. This is because both g_{ct}^R and $\Delta g_{sb(ds)}^L$ are proportional to m_U^{-2} , up to logarithmic dependence, multiplied by a quadratic form in Y_{Ut} and Y_{Uc} [See Eqs. (7) and (43)]. Thus, changing m_U simply results in rescaled Y_{Ut} and Y_{Uc} values. A similar argument applies to the dependence on the $U(1)'$ coupling g' .

As we took $Y_{Uu} = 0$ to avoid D meson constraints, one might think that $Y_{Ut} > Y_{Uc} > Y_{Uu}$ is the natural ordering of these Yukawa couplings. Taking $Y_{Ut} = 1$ and $Y_{Uc} = \lambda$, we plot in Fig. 6 [left] $\mathcal{B}(t \rightarrow cZ')_{\text{RH}}$ as a function of m_U for $m_{Z'} = 334$ MeV, with B and K constraints overlaid. In this case, the LHCb constraint is severe, implying $\mathcal{B}(t \rightarrow cZ')_{\text{RH}} \lesssim 0.6 \times 10^{-10}$. A similar plot for $m_{Z'} = 219$ MeV is given in Fig. 6 [right], where the LHCb limit implies $\mathcal{B}(t \rightarrow cZ')_{\text{RH}} \lesssim 2 \times 10^{-10}$. The pocket 211.3 MeV $\lesssim m_{Z'} < 212$ MeV is still constrained by E949, giving $\mathcal{B}(t \rightarrow cZ')_{\text{RH}} \lesssim 3 \times 10^{-9}$.

In short, for the hierarchical Yukawa couplings $Y_{Ut} = 1$, $Y_{Uc} = \lambda$, we obtain $\mathcal{B}(t \rightarrow cZ')_{\text{RH}} \lesssim \mathcal{O}(10^{-9})$ in the whole mass range of Scenario (ii-a), namely $2m_\mu < m_{Z'} \lesssim 400$ MeV. These values seem beyond reach of the LHC. On the other hand, if Y_{Ut} and Y_{Uc} are treated as free parameters, $\mathcal{B}(t \rightarrow cZ')_{\text{RH}}$ can be much larger. In particular, $\mathcal{B}(t \rightarrow cZ')_{\text{RH}} \sim \mathcal{O}(10^{-5})$ is possible in the funnel regions for appropriately high Z' masses such that the E949 limit is weakened. This may be within reach at the future LHC, as shown in Eq. (26), but a fine-tuned correlation between Y_{Ut} and Y_{Uc} would be needed. Note that our projection for LHC sensitivities is rather naive. A careful collider study should be done to judge the actual sensitivity for $t \rightarrow cZ'$ at the LHC.

Surveying other $m_{Z'}$ cases, we find the constraints on $\mathcal{B}(t \rightarrow cZ')_{\text{RH}}$ in Scenario (ii-a) can be classified into the following three categories.

- 330 MeV $\lesssim m_{Z'} \lesssim 400$ MeV:
 $\mathcal{B}(t \rightarrow cZ')_{\text{RH}} \gtrsim 10^{-6}$ is possible along the funnel regions allowed by hidden-sector boson search of LHCb in $B^0 \rightarrow K^{*0} \chi (\rightarrow \mu^+ \mu^-)$. In particular, if $m_{Z'} \gtrsim m_{K^+} - m_{\pi^+} \simeq 354$ MeV, the K^+ decay constraints can be avoided, and $\mathcal{B}(t \rightarrow cZ')_{\text{RH}}$ may be arbitrary large for large Y_{Uc} , up to perturbativity and associated fine-tuning of Y_{Ut} .
- 230 MeV $\lesssim m_{Z'} \lesssim 330$ MeV:

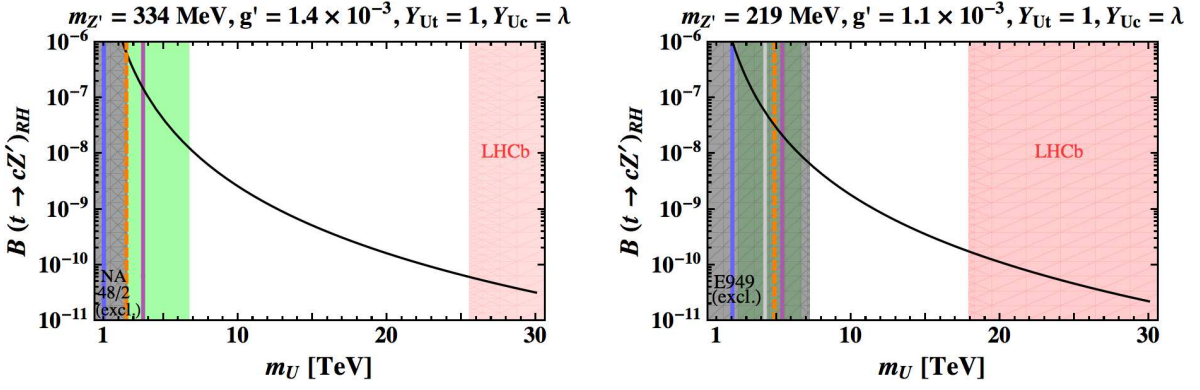


FIG. 6. [Left] Branching ratio $\mathcal{B}(t \rightarrow cZ')_{\text{RH}}$ of right-handed current mediated $t \rightarrow cZ'$ as a function of vector-like quark mass m_U for $m_{Z'} = 334$ MeV and $g' = 1.4 \times 10^{-3}$ with hierarchical Yukawa couplings $Y_{Ut} = 1$, $Y_{Uc} = \lambda \simeq 0.23$. Shaded regions and lines are constraints on m_U from B and K decay data, with the shadings and lines as explained in Fig. 5. [Right] Same as left panel, but for $m_{Z'} = 219$ MeV and $g' = 1.1 \times 10^{-3}$.

$\mathcal{B}(t \rightarrow cZ')_{\text{RH}} \gtrsim 10^{-6}$ is possible along the funnel regions, but $K^+ \rightarrow \pi^+ \mu^+ \mu^-$ (NA48/2) and/or $K^+ \rightarrow \pi^+ P^0 (\rightarrow \nu \bar{\nu})$ (E949) constraints cut in, such that $\mathcal{B}(t \rightarrow cZ')_{\text{RH}} \lesssim 10^{-5}$.

- $2m_\mu < m_{Z'} \lesssim 230$ MeV:

The E949 limit gets stronger towards $m_{Z'} = 2m_\mu$, fully excluding the funnel regions, giving $\mathcal{B}(t \rightarrow cZ')_{\text{RH}} \lesssim 10^{-6}$, even in the 211.3 MeV $\lesssim m_{Z'} < 212$ MeV pocket, where neither LHCb nor Belle limits for $B^0 \rightarrow K^{*0} Z' (\rightarrow \mu^+ \mu^-)$ apply.

We have ignored the interference of Z' effect with SM contribution, as the Z' width is tiny. We remark, however, that for $m_{Z'} > 2m_\pi$, an absorptive part of $K^+ \rightarrow \pi^+ \gamma^* (\rightarrow \mu^+ \mu^-)$ induced by the $\pi\pi$ loop may invalidate the simple separation of SM and Z' contributions to $K^+ \rightarrow \pi^+ \mu^+ \mu^-$. This might affect the second mass range, in particular the position where the funnels are cut down by the NA48/2 limit.

IV. A LIGHT Z' THAT EVADES GROSSMAN-NIR BOUND

In this section, we study the scenario where

$$m_{Z'} < 2m_\mu \quad [\text{Scenario (ii-b)}]. \quad (54)$$

In this case, the Z' bosons decay exclusively into neutrino pairs and are just felt as missing energy in collider experiments. As such, it would be more challenging to search for $t \rightarrow cZ'$ at the LHC. Nevertheless, we estimate for completeness the allowed ranges for $t \rightarrow cZ'$ branching ratios via left- or right-handed current in this scenario. The relevant formulas and meson decay constraints were already summarized in the previous section.

An interesting outcome of this scrutiny is the possibility, pointed out by us previously [22], that an invisible Z' boson could evade the commonly accepted Grossman-Nir (GN) bound [23] of $\mathcal{B}(K_L \rightarrow \pi^0 \nu \bar{\nu}) \lesssim 1.4 \times 10^{-9}$.

A. $t \rightarrow cZ' (\rightarrow \nu \bar{\nu})$ via left-handed current

We use BaBar data on $B \rightarrow K^{(*)} \nu \bar{\nu}$ in Eq. (37) to constrain the tree-level effective bsZ' couplings g_{sb}^L and g_{sb}^R . The 2σ range for $B^+ \rightarrow K^+ \nu \bar{\nu}$ imposes

$$0.16 \times 10^{-9} \lesssim |g_{sb}^L + g_{sb}^R| \left(\frac{100 \text{ MeV}}{m_{Z'}} \right) \lesssim 0.88 \times 10^{-9}, \quad (55)$$

while the $B^+ \rightarrow K^{*+} \nu \bar{\nu}$ data mainly constrains the other combination of the bsZ' couplings,

$$|g_{sb}^L - g_{sb}^R| \left(\frac{100 \text{ MeV}}{m_{Z'}} \right) \lesssim 1.3 \times 10^{-9}. \quad (56)$$

Combining the two constraints, we get

$$|g_{sb}^L|, |g_{sb}^R| \lesssim 1.1 \times 10^{-9} \left(\frac{m_{Z'}}{100 \text{ MeV}} \right), \quad (57)$$

for $m_{Z'} < 2m_\mu$. Note that the excess in the $B^+ \rightarrow K^{*+} \nu \bar{\nu}$ data does not necessarily imply a nonzero g_{sb}^L , as $g_{sb}^L = 0$ can still explain the excess by a nonzero g_{sb}^R .

Using the $SU(2)_L$ relation $g_{ct}^L \simeq g_{sb}^L$, we obtain the upper limit on the left-handed current contribution to the $t \rightarrow cZ'$ branching ratio,

$$\mathcal{B}(t \rightarrow cZ')_{\text{LH}} \lesssim 4 \times 10^{-12} \quad (58)$$

for $m_{Z'} < 2m_\mu$. Note that the limit does not depend on $m_{Z'}$, as it cancels out in the final expression.

B. $t \rightarrow cZ' (\rightarrow \nu \bar{\nu})$ via right-handed current

We constrain the right-handed current contribution to the $t \rightarrow cZ'$ branching ratio by using $B^+ \rightarrow K^+ \nu \bar{\nu}$ and $K \rightarrow \pi \nu \bar{\nu}$ data. As discussed in the previous section, the E949 constraint from $K^+ \rightarrow \pi^+ P^0 (\rightarrow \nu \bar{\nu})$ search can

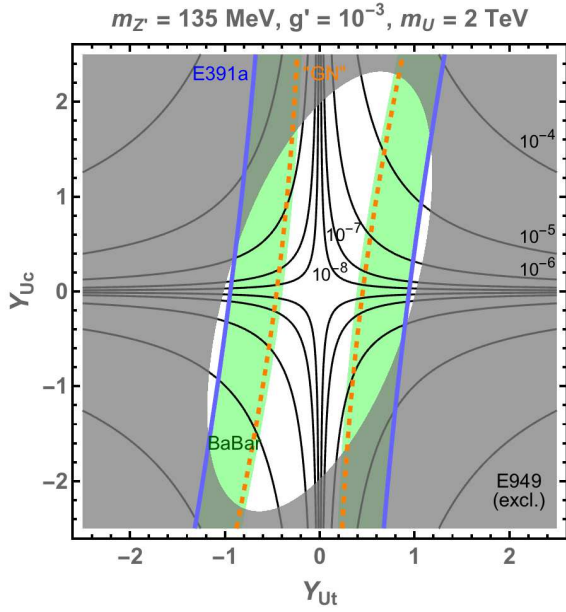


FIG. 7. Same as Fig. 5 [right], but for $m_{Z'} = 135$ MeV and $g' = 10^{-3}$, with the E949 exclusion of Eq. (51).

be avoided, if the Z' mass falls into the π^0 -mass window, i.e. $125 \text{ MeV} \lesssim m_{Z'} \lesssim 150 \text{ MeV}$. Although this mass window is still constrained by $\pi^0 \rightarrow \nu\bar{\nu}$, searched in $K^+ \rightarrow \pi^+\pi^0$ [Eq. (51)], the limit is rather weak compared to the $K^+ \rightarrow \pi^+P^0(\rightarrow \nu\bar{\nu})$ limits outside the π^0 -window. [See explanation below Eq. (50).] To allow for the possibility of a large $t \rightarrow cZ'$ rate, we take the following benchmark point:

- $m_{Z'} = 135 \text{ MeV}$, $g' = 10^{-3}$, $m_U = 2 \text{ TeV}$,

which is shown by a red cross in Fig. 3. The B and K decay constraints are summarized in Table I. As discussed in the previous section, this particular choice of g' and m_U does not affect the final result for $\mathcal{B}(t \rightarrow cZ')_{\text{RH}}$.

In Fig. 7, we give contours of $\mathcal{B}(t \rightarrow cZ')_{\text{RH}}$ as black-solid lines in the (Y_{Ut}, Y_{Uc}) plane. The B and K decay constraints are overlaid with the shadings and line styles as in Fig. 5 [right]. The semi-transparent dark-gray shaded region is excluded by the E949 limit on $\pi^0 \rightarrow \nu\bar{\nu}$ at 90% C.L. [Eq. (51)]. In the present case, the E391a constraint on $K_L \rightarrow \pi^0\nu\bar{\nu}$ [Eq. (52)], shown as blue-solid lines, also plays a role. The green shaded regions, favored by the mild $B^+ \rightarrow K^+\nu\bar{\nu}$ excess in BaBar data [in Eq. (37)], are compatible with other constraints in most parts of the shown range. This is in contrast to Scenario (ii-a), where the constraints from $B^0 \rightarrow K^{*0}\chi(\rightarrow \mu^+\mu^-)$ and $K^+ \rightarrow \pi^+P^0(\rightarrow \nu\bar{\nu})$ exclude the BaBar regions. In this benchmark point, we obtain $\mathcal{B}(t \rightarrow cZ')_{\text{RH}} \lesssim 5 \times 10^{-5}$.

Fixing the Yukawa couplings to $Y_{Ut} = 1$, $Y_{Uc} = \lambda$, we plot $\mathcal{B}(t \rightarrow cZ')_{\text{RH}}$ in Fig. 8 as a function of m_U with the same $m_{Z'}$ and g' values. For this case, the BaBar excess favors a nonzero but small $t \rightarrow cZ'$ rate within $6 \times 10^{-9} \lesssim \mathcal{B}(t \rightarrow cZ')_{\text{RH}} \lesssim 5 \times 10^{-7}$.

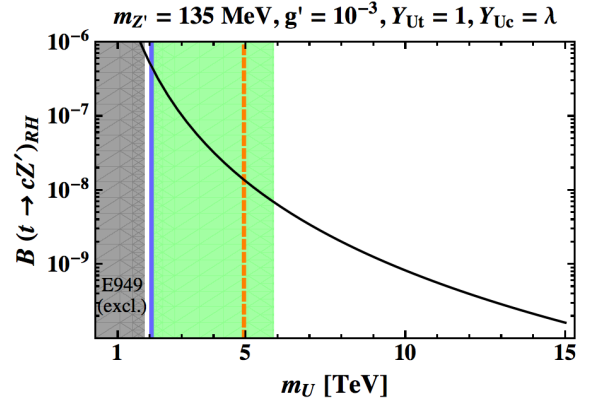


FIG. 8. Same as Fig. 6 [right], but for $m_{Z'} = 135$ MeV and $g' = 10^{-3}$.

For the Z' mass within the π^0 -window, i.e. $125 \text{ MeV} \lesssim m_{Z'} \lesssim 150 \text{ MeV}$, the same E949 limit for $K^+ \rightarrow \pi^+Z'$ applies and we obtain similar results for $\mathcal{B}(t \rightarrow cZ')_{\text{RH}}$.

The E949 limit gets stronger considerably if the Z' mass is out of the π^0 -window, hence $\mathcal{B}(t \rightarrow cZ')_{\text{RH}}$ cannot be larger than the above limits. For instance, taking $m_{Z'} = 11 \text{ MeV}$ with $g' = 5 \times 10^{-4}$, motivated by IceCube data [24, 63], we obtain $\mathcal{B}(t \rightarrow cZ')_{\text{RH}} \lesssim 6 \times 10^{-8}$.

In summary, we obtain $\mathcal{B}(t \rightarrow cZ')_{\text{RH}} \lesssim 5 \times 10^{-5}$ for any $m_{Z'}$ in Scenario (ii-b). The decay $t \rightarrow cZ'(\rightarrow \nu\bar{\nu})$ at 100% with such a small branching ratio might be quite challenging for searches at the LHC.

C. Apparent violation of Grossman-Nir bound

The light Z' has an interesting implication for kaon decay experiments [22].

From isospin symmetry, the branching ratio $\mathcal{B}(K_L \rightarrow \pi^0\nu\bar{\nu})$ is connected with $\mathcal{B}(K^+ \rightarrow \pi^+\nu\bar{\nu})$ by a *model-independent* relation, known as the Grossman-Nir (GN) bound [23],

$$\mathcal{B}(K_L \rightarrow \pi^0\nu\bar{\nu}) \lesssim 4.3 \times \mathcal{B}(K^+ \rightarrow \pi^+\nu\bar{\nu}), \quad (59)$$

where the overall factor of 4.3 comes from $\tau_{K_L}/\tau_{K^+} \simeq 4.1$ and isospin-breaking effects. Plugging in the 90% C.L. upper limit of $\mathcal{B}(K^+ \rightarrow \pi^+\nu\bar{\nu}) < 3.35 \times 10^{-10}$ by E949 [60], the GN bound leads to

$$\mathcal{B}(K_L \rightarrow \pi^0\nu\bar{\nu}) \lesssim 1.4 \times 10^{-9}. \quad (\text{“GN”}) \quad (60)$$

This is an order of magnitude stronger than the direct limit on $K_L \rightarrow \pi^0\nu\bar{\nu}$ by E391a, Eq. (52). In Figs. 5–8, this commonly accepted GN bound is shown by the orange-dashed lines.

There are two ongoing experiments in search for $K \rightarrow \pi\nu\bar{\nu}$ decays. The NA62 experiment [66] at CERN aims at measuring of order 100 $K^+ \rightarrow \pi^+\nu\bar{\nu}$ events, while the KOTO experiment [67] at J-PARC aims at 3σ measurement of $K_L \rightarrow \pi^0\nu\bar{\nu}$ at SM rate. KOTO has already

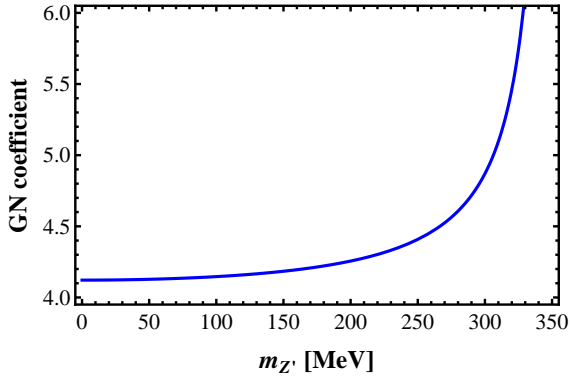


FIG. 9. Maximally allowed value as a function of $m_{Z'}$ for ratio $\mathcal{B}(K_L \rightarrow \pi^0 Z')/\mathcal{B}(K^+ \rightarrow \pi^+ Z')$, given in Eq. (61).

reached [68] the sensitivity of E391a [Eq. (52)], but folklore is that KOTO can start to probe New Physics effects only after Eq. (60) is breached.

We have argued, however, that the kinematic selection in $K^+ \rightarrow \pi^+ \nu \bar{\nu}$ searches (including both E949 and NA62) makes them insensitive to the possible existence of a light new boson X^0 , produced in $K^+ \rightarrow \pi^+ X^0$, if $m_{X^0} \sim m_\pi$ or larger than $2m_\pi$. If so, the usual GN bound of Eq. (60) does not apply, and therefore, without such a selection, KOTO is already entering the domain of New Physics.

A relation similar to Eq. (59) still holds for the light Z' contribution, with a slight modification in the overall coefficient. Taking the ratio of the $K_L \rightarrow \pi^0 Z'$ and $K^+ \rightarrow \pi^+ Z'$ branching ratios in Eq. (46), we obtain the light Z' version of the GN bound:

$$\begin{aligned} \frac{\mathcal{B}(K_L \rightarrow \pi^0 Z')}{\mathcal{B}(K^+ \rightarrow \pi^+ Z')} &= \frac{\tau_{K_L}}{\tau_{K^+}} \frac{1}{r(m_{Z'}^2)} \left| \frac{\text{Im}(g_{ds}^L + g_{ds}^R)}{g_{ds}^L + g_{ds}^R} \right|^2 \\ &\leq \frac{\tau_{K_L}}{\tau_{K^+}} \frac{1}{r(m_{Z'}^2)}, \end{aligned} \quad (61)$$

where the isospin breaking factor $r(m_{Z'}^2)$ is defined by

$$\frac{1}{r(m_{Z'}^2)} \equiv \frac{m_{K_L}^3 \beta_{K_L \pi^0 Z'}^3}{m_{K^+}^3 \beta_{K^+ \pi^+ Z'}^3} \left[\frac{f_+^{K^0 \pi^0}(m_{Z'}^2)}{f_+^{K^+ \pi^+}(m_{Z'}^2)} \right]^2. \quad (62)$$

To keep generality, we recover the dependence on g_{ds}^R , assuming the interaction form of Eq. (6). The form factor ratio is known to be q^2 -independent at next-to-leading order in chiral perturbation theory, with numerical value $f_+^{K^+ \pi^+}(q^2)/f_+^{K^0 \pi^0}(q^2) = 1.0238 \pm 0.0022$ [53]. The genuine GN bound of Eq. (61) is then given by

$$\frac{\mathcal{B}(K_L \rightarrow \pi^0 Z')}{\mathcal{B}(K^+ \rightarrow \pi^+ Z')} \lesssim 4.122 \left(\frac{1.003}{r(m_{Z'}^2)} \right), \quad (63)$$

where $r(0) = 1.003$ is taken as reference. The right-hand side, the ‘‘GN coefficient’’, depends on the Z' mass, as illustrated in Fig. 9.

For 125 MeV $\lesssim m_{Z'} \lesssim 150$ MeV, plugging in the 90% C.L. upper limit on $\mathcal{B}(K^+ \rightarrow \pi^+ Z')$ by E949 [Eq. (51)],

we obtain $\mathcal{B}(K_L \rightarrow \pi^0 Z') \lesssim 2.3 \times 10^{-7}$. The direct bound on $K_L \rightarrow \pi^0 \nu \bar{\nu}$ by E391a, Eq. (52), is indeed stronger than this true GN bound.

The above argument is general and applicable to any weakly interacting light boson, or short-lived invisibly decaying boson, that couples to $s \rightarrow d$ currents. The bound of Eq. (61) holds for a massive vector boson that couples to the $s \rightarrow d$ currents in the form of Eq. (6). On the other hand, for the $L_\mu - L_\tau$ gauge boson with loop-induced sdZ' coupling of Eq. (43), we obtain $|\text{Im}(\Delta g_{ds}^L)/g_{ds}^L|^2 \sim |\text{Im}(V_{ts} V_{td}^*)/(V_{ts} V_{td}^*)|^2 \simeq 0.15$, as long as $Y_{Ut} \gtrsim Y_{Uc}$, due to top-top dominance in loop. Thus, the GN bound of Eq. (61) cannot be saturated in this case.

The argument can be further extended to three-body kaon decays where the final state contains a pair of new massive invisible particles (χ), i.e., $K \rightarrow \pi \chi \chi$. If the mass of χ is larger than m_π , the decay is allowed only if the invariant mass of the χ pair satisfies $2m_\pi < m_{\chi\chi} (< m_K - m_\pi)$. In this case, the π^+ momentum is always outside the signal regions of the $K^+ \rightarrow \pi^+ \nu \bar{\nu}$ experiments, hence, the usual GN bound does not apply. An interesting candidate is the very light neutralino in the minimal supersymmetric standard model, which was discussed in Ref. [64], although the analysis needs to be updated in light of recent LHC results. (See Ref. [65] for recent assessment of the light neutralino.)

V. DISCUSSION AND CONCLUSIONS

The so-called P'_5 and R_K anomalies in $b \rightarrow s$ transitions, as revealed by LHCb data, suggest the possible existence of a new massive gauge boson Z' coupling to left-handed $b \rightarrow s$ current, which in turn implies tcZ' coupling. Motivated by this, we studied the top FCNC decay $t \rightarrow cZ'$ based on the gauged $L_\mu - L_\tau$ model with vector-like quarks that mix with SM quarks. The model can also be applied to address the muon $g-2$ anomaly, which turns out to allow only a very light Z' due to neutrino scattering data. The situation is mutually exclusive with the $b \rightarrow s$ anomalies. We studied how large the $t \rightarrow cZ'$ rate can be in three well-motivated scenarios: (i) heavy Z' with $m_b \lesssim m_{Z'} < m_t - m_c$, motivated by the P'_5 and R_K anomalies; (ii-a) light Z' with $2m_\mu < m_{Z'} \lesssim 400$ MeV, motivated by the muon $g-2$ anomaly; (ii-b) the $(g-2)_\mu$ -motivated Z' with $m_{Z'} < 2m_\mu$.

In Scenario (i), using a global fit result of $b \rightarrow s$ data as well as B_s meson mixing constraint, we find that the left-handed current contribution to branching ratio $\mathcal{B}(t \rightarrow cZ')_{\text{LH}}$ can be as large as 10^{-6} . We also find that the right-handed current contribution $\mathcal{B}(t \rightarrow cZ')_{\text{RH}}$, which is not constrained by B data, can be as large as $\mathcal{O}(10^{-4})$ with reasonably large mixing (around the Cabibbo angle) between vector-like quark U and t, c . The left-handed case would be beyond the reach of even the high-luminosity LHC upgrade, while the right-handed case might be accessible already with LHC Run 1 data. [See Eq. (26) for our naive projection based on $t \rightarrow qZ$

results.]

In Scenario (ii-a), we find $\mathcal{B}(t \rightarrow cZ')_{\text{LH}}$ to be extremely tiny, below 10^{-11} , due to rare B decay constraints. In this scenario, even the right-handed current contribution is constrained by rare B and K decays via one-loop effects. We find that $\mathcal{B}(t \rightarrow cZ')_{\text{RH}} \gtrsim 10^{-6}$ is allowed only at the cost of fine-tuning the relation between Y_{Ut} and Y_{Uc} . Nevertheless, in such cancellation regions, $\mathcal{B}(t \rightarrow cZ')_{\text{RH}}$ may be larger than $\mathcal{O}(10^{-5})$ for $330 \text{ MeV} \lesssim m_{Z'} \lesssim 400 \text{ MeV}$. Our naive projection based on $t \rightarrow qZ$ results suggests that this could be within reach of the ATLAS and CMS experiments with 300^{-1} data at the (13-)14 TeV LHC. However, a careful collider study is needed to find the true sensitivity, as the search strategy needs to be changed from the $t \rightarrow qZ$ case.

Scenario (ii-b) can accommodate larger $t \rightarrow cZ'$ branching ratios for the right-handed current contribution: $\mathcal{B}(t \rightarrow cZ')_{\text{RH}} \lesssim 5 \times 10^{-5}$. This case, however, would be more challenging for collider search, as the Z' decays exclusively into neutrinos (but with little missing mass). Such a light Z' is interesting instead for rare kaon decay experiments, and could even lead to observation of New Physics beyond the so-called Grossman-Nir bound, or $\mathcal{B}(K_L \rightarrow \pi^0 + \text{nothing}) > 1.4 \times 10^{-9}$. If this happens, our prediction is that it occurs via $K_L \rightarrow \pi^0 X^0$ with unobserved $m_{X^0} \sim m_{\pi^0}$, with our Z' motivated by muon $g - 2$ as a candidate. We remark that the Z' in Scenarios (ii-a) and (ii-b) may also be probed by the future neutrino beam facility LBNE [69] via neutrino trident production [21]. And certainly LHCb and Belle II experiments should pursue further ‘‘bump’’ searches in $B \rightarrow K^{(*)}\mu^+\mu^-$ and $B \rightarrow K^{(*)}\nu\bar{\nu}$ decays.

In this paper, we assumed a particular Z' model to study $t \rightarrow cZ'$ decay. In the model, the right-handed tcZ' coupling correlates with the ttZ' and ccZ' couplings. In particular, the ttZ' coupling is strongly constrained by loop-induced decays from chiral m_t/m_c enhancement, and the tcZ' coupling in turn is also constrained indirectly. This correlation is not general, and the meson decay constraints might be relaxed in some other Z' models where the right-handed tcZ' coupling is independent from the ttZ' coupling.

The muon $g - 2$ anomaly implies that the $U(1)'$ symmetry breaking scale v_Φ is around the electroweak scale of 246 GeV or below. The mass of the new Higgs boson ϕ behind the spontaneous breaking of the $U(1)'$ symmetry, is hence expected to be below 1 TeV and within reach at the LHC. The mixing of the vector-like U quark with top via the ϕ -Yukawa interaction leads to effective $tt\phi$ coupling. Thus, the ϕ can be produced via gluon fusion $gg \rightarrow \phi$, followed by $\phi \rightarrow Z'Z'(\rightarrow 4\mu/2\mu 2\nu)$, as pointed out in Ref. [22]. The effective $tt\phi$ coupling, however, is highly suppressed compared to the SM top Yukawa coupling, due to the constraints from $B^0 \rightarrow K^{*0}Z'(\rightarrow \mu^+\mu^-)$ as discussed in Sec. II, hence the $gg \rightarrow \phi$ cross section is too small to be observed at the LHC [26]. Instead, the effective $tc\phi$ couplings, generated in a similar way as tcZ' , may offer another ϕ production mechanism,

i.e. $t \rightarrow c\phi$ in $t\bar{t}$ events at the LHC. This gives rise to a striking signature, namely two collimated dimuons in $pp \rightarrow t\bar{t} \rightarrow bWc\phi(\rightarrow Z'Z')$ with $Z'Z' \rightarrow (\mu^+\mu^-)(\mu^+\mu^-)$. This interesting possibility will be pursued elsewhere [26].

Acknowledgement. KF is supported by Research Fellowships of the Japan Society for the Promotion of Science for Young Scientists, No. 15J01079. WSH is supported by the Academic Summit grant MOST 103-2745-M-002-001-ASP of the Ministry of Science and Technology, as well as by grant NTU-EPR-103R8915. MK is supported under NSC 102-2112-M-033-007-MY3. MK thanks Y. Chao, A. Mauri, J. Tandean and M. Williams for valuable discussions. WSH thanks T. Blake and M. Pepe-Altarelli for correspondence. KF thanks useful correspondence with S. Gori, and the NTUHEP group for hospitality during exchange visits.

Appendix A: Efficiency for $B^0 \rightarrow K^{*0}Z' \rightarrow K\pi\mu^+\mu^-$

In order to estimate the efficiency for the $B^0 \rightarrow K^{*0}Z' \rightarrow K\pi\mu^+\mu^-$ decay at the LHCb, we need information of the angular distribution for this decay. In the narrow width approximation, the normalized differential decay width for $\bar{B}^0 \rightarrow \bar{K}^{*0}Z' \rightarrow K^-\pi^+\mu^+\mu^-$ is given by

$$\begin{aligned} & \frac{1}{\Gamma} \frac{d\Gamma}{d \cos \theta_K d \cos \theta_\ell d\phi} \\ &= \frac{9}{16\pi(1 + 2m_\mu^2/m_{Z'}^2)(|H_0|^2 + |H_+|^2 + |H_-|^2)} \\ & \times \left\{ -\beta_\mu^2 \left[|H_0|^2 \cos^2 \theta_K \cos^2 \theta_\ell \right. \right. \\ & \left. \left. + \frac{1}{4}(|H_+|^2 + |H_-|^2) \sin^2 \theta_K \sin^2 \theta_\ell + \Xi(\theta_K, \theta_\ell, \phi) \right] \right. \\ & \left. + |H_0|^2 \cos^2 \theta_K + \frac{1}{2}(|H_+|^2 + |H_-|^2) \sin^2 \theta_K \right\}, \quad (\text{A1}) \end{aligned}$$

where $\beta_\mu \equiv \sqrt{1 - 4m_\mu^2/m_{Z'}^2}$ and the helicity amplitudes $H_{0,\pm}$ are given in Eq. (32). The ϕ -dependence enters solely through the function

$$\begin{aligned} & \Xi(\theta_K, \theta_\ell, \phi) \\ &= -\frac{1}{4} \sin 2\theta_K \sin 2\theta_\ell \{ \cos \phi [\text{Re}(H_0 H_+^*) + \text{Re}(H_0 H_-^*)] \\ & \quad - \sin \phi [\text{Im}(H_0 H_+^*) - \text{Im}(H_0 H_-^*)] \} + \frac{1}{2} \sin^2 \theta_K \sin^2 \theta_\ell \\ & \quad \times [\cos 2\phi \text{Re}(H_+ H_-^*) + \sin 2\phi \text{Im}(H_+ H_-^*)]. \quad (\text{A2}) \end{aligned}$$

We follow the LHCb convention [70] for the definition of decay angles: θ_ℓ is the angle between direction of μ^- and direction opposite to \bar{B}^0 in the Z' rest frame; θ_K is the angle between direction of K^- and direction opposite to \bar{B}^0 in the \bar{K}^{*0} rest frame; ϕ is the angle between $Z' \rightarrow \mu^+\mu^-$ decay plane and $K^{*0} \rightarrow K^-\pi^+$ decay plane in the \bar{B}^0 rest frame.

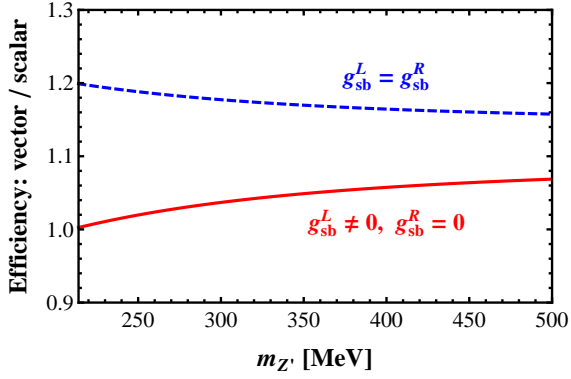


FIG. 10. Ratio of efficiencies between vector-boson Z' and scalar-boson χ for $\bar{B}^0 \rightarrow \bar{K}^{*0} Z'(\chi) \rightarrow K^- \pi^+ \mu^+ \mu^-$ events collected by LHCb. Solid line is for $g_{sb}^L \neq 0$, $g_{sb}^R = 0$ and dashed line is for $g_{sb}^L = g_{sb}^R$. The other two cases of $g_{sb}^L = 0$, $g_{sb}^R \neq 0$ and $g_{sb}^L = -g_{sb}^R$ behave similarly to the solid line.

If a new scalar-boson χ mediates the four-body decay instead of the vector-boson Z' , the angular distribution simply behaves as $d\Gamma/d\cos\theta_K d\cos\theta_\ell d\phi \propto \cos^2\theta_K$. This is the case assumed in the LHCb search [45] for hidden-sector bosons χ in $B^0 \rightarrow K^{*0}\chi$. In order to convert the limits on $B^0 \rightarrow K^{*0}\chi$ into the Z' case, one needs to know the ratio of the efficiencies between the χ and Z' cases. Ref. [45] (see Supplemental Material) provides this information in the form of ratio between integrals of the trigonometric functions appearing in Eq. (A1) and integral of $\cos^2\theta_K$, taking into account the efficiency. Using this information, we obtain the ratio of efficiencies for Z' to χ , as shown in Fig. 10. For $g_{sb}^R = 0$, corresponding to the loop-induced coupling discussed in Sec. III, the change in efficiencies from the scalar case is within 6% for $m_{Z'} \leq 400$ MeV. If we allow general chiral structure for bsZ' coupling, the change is still small, within 20% for $m_{Z'} \leq 400$ MeV.

Appendix B: Loop functions for effective couplings

The loop functions given in Eq. (45) are approximate formulas in the large m_U limit. In our numerical study, we use the following expression:

$$f_{qq'} = -4m_W^2 m_U^4 I_0^{qq'} + (2m_W^2 + m_U^2) m_U^2 I_2^{qq'} - 2m_U^2 I_4^{qq'}, \quad (\text{B1})$$

where $q, q' = t, c$, and

$$\begin{aligned} I_0^{qq'} &\equiv \int \frac{d^4k}{i(2\pi)^4} \frac{16\pi^2}{(k^2 - m_q^2)(k^2 - m_{q'}^2)(k^2 - m_U^2)^2(k^2 - m_W^2)} \\ &= - \int_0^1 dx_1 \int_0^{1-x_1} dx_2 \frac{(1-x_1-x_2)^2}{\alpha_{qq'} \beta_{qq'}^2}, \end{aligned} \quad (\text{B2})$$

$$\begin{aligned} I_2^{qq'} &\equiv \int \frac{d^4k}{i(2\pi)^4} \frac{16\pi^2 k^2}{(k^2 - m_q^2)(k^2 - m_{q'}^2)(k^2 - m_U^2)^2(k^2 - m_W^2)} \\ &= \frac{2}{(m_U^2 - m_W^2)^2} \int_0^1 dx_1 \int_0^{1-x_1} dx_2 \\ &\quad \times \left[\ln \frac{\beta_{qq'}}{\alpha_{qq'}} - \frac{(1-x_1-x_2)(m_U^2 - m_W^2)}{\beta_{qq'}} \right], \end{aligned} \quad (\text{B3})$$

$$\begin{aligned} I_4^{qq'} &\equiv \int \frac{d^4k}{i(2\pi)^4} \frac{16\pi^2 (k^2)^2}{(k^2 - m_q^2)(k^2 - m_{q'}^2)(k^2 - m_U^2)^2(k^2 - m_W^2)} \\ &= - \frac{6}{m_U^2 - m_W^2} \int_0^1 dx_1 \int_0^{1-x_1} dx_2 \\ &\quad \times \left(1 - x_1 - x_2 - \frac{\alpha_{qq'}}{m_U^2 - m_W^2} \ln \frac{\beta_{qq'}}{\alpha_{qq'}} \right), \end{aligned} \quad (\text{B4})$$

with

$$\begin{aligned} \alpha_{qq'} &= x_1 m_q^2 + x_2 m_{q'}^2 + (1-x_1-x_2) m_W^2, \\ \beta_{qq'} &= x_1 m_q^2 + x_2 m_{q'}^2 + (1-x_1-x_2) m_U^2. \end{aligned} \quad (\text{B5})$$

-
- [1] K.A. Olive *et al.* [Particle Data Group], *Chin. Phys. C* **38**, 090001 (2014).
[2] R. Aaij *et al.* [LHCb Collaboration], *Phys. Rev. Lett.* **111**, 191801 (2013) [arXiv:1308.1707 [hep-ex]].
[3] LHCb Collaboration, LHCb-CONF-2015-002; R. Aaij *et al.* [LHCb Collaboration], *JHEP* **1602**, 104 (2016) [arXiv:1512.04442 [hep-ex]].
[4] R. Aaij *et al.* [LHCb Collaboration], *Phys. Rev. Lett.* **113**, 151601 (2014) [arXiv:1406.6482 [hep-ex]].
[5] S. Descotes-Genon, J. Matias, J. Virto, *Phys. Rev. D* **88**, 074002 (2013) [arXiv:1307.5683 [hep-ph]].
[6] W. Altmannshofer and D.M. Straub, *Eur. Phys. J. C* **73**, 2646 (2013) [arXiv:1308.1501 [hep-ph]].
[7] F. Beaujean, C. Bobeth, D. van Dyk, *Eur. Phys. J. C* **74**, 2897 (2014) [Erratum *Eur. Phys. J. C* **74**, 3179 (2014)] [arXiv:1310.2478 [hep-ph]].
[8] R.R. Horgan, Z. Liu, S. Meinel, M. Wingate, *Phys. Rev. Lett.* **112**, 212003 (2014) [arXiv:1310.3887 [hep-ph]].
[9] T. Hurth and F. Mahmoudi, *JHEP* **1404**, 097 (2014) [arXiv:1312.5267 [hep-ph]].
[10] R. Alonso, B. Grinstein, J.M. Camalich, *Phys. Rev. Lett.* **113**, 241802 (2014) [arXiv:1407.7044 [hep-ph]].

- [11] G. Hiller and M. Schmaltz, Phys. Rev. D **90**, 054014 (2014) [arXiv:1408.1627 [hep-ph]].
- [12] D. Ghosh, M. Nardecchia, S.A. Renner, JHEP **1412**, 131 (2014) [arXiv:1408.4097 [hep-ph]].
- [13] T. Hurth, F. Mahmoudi, S. Neshatpour, JHEP **1412**, 053 (2014) [arXiv:1410.4545 [hep-ph]].
- [14] W. Altmannshofer and D.M. Straub, Eur. Phys. J. C **75**, 382 (2015) [arXiv:1411.3161 [hep-ph]].
- [15] W. Altmannshofer, S. Gori, M. Pospelov, I. Yavin, Phys. Rev. D **89**, 095033 (2014) [arXiv:1403.1269 [hep-ph]].
- [16] X.-G. He, G.C. Joshi, H. Lew, R.R. Volkas, Phys. Rev. D **43**, 22 (1991).
- [17] P.J. Fox, J. Liu, D. Tucker-Smith, N. Weiner, Phys. Rev. D **84**, 115006 (2011) [arXiv:1104.4127 [hep-ph]].
- [18] The $t \rightarrow uZ'$ decay with a hadronically decaying Z' was discussed in S. Jung, H. Murayama, A. Pierce, J.D. Wells, Phys. Rev. D **81**, 015004 (2010) [arXiv:0907.4112 [hep-ph]].
- [19] F. Jegerlehner and A. Nyffeler, Phys. Rept. **477**, 1 (2009) [arXiv:0902.3360 [hep-ph]].
- [20] S. Baek, N.G. Deshpande, X.-G. He, P. Ko, Phys. Rev. D **64**, 055006 (2001) [hep-ph/0104141].
- [21] W. Altmannshofer, S. Gori, M. Pospelov, I. Yavin, Phys. Rev. Lett. **113**, 091801 (2014) [arXiv:1406.2332 [hep-ph]].
- [22] K. Fuyuto, W.-S. Hou, M. Kohda, Phys. Rev. Lett. **114**, 171802 (2015) [arXiv:1412.4397 [hep-ph]].
- [23] Y. Grossman and Y. Nir, Phys. Lett. B **398**, 163 (1997) [hep-ph/9701313].
- [24] T. Araki, F. Kaneko, Y. Konishi, T. Ota, J. Sato, T. Shimomura, Phys. Rev. D **91**, 037301 (2015) [arXiv:1409.4180 [hep-ph]].
- [25] M.G. Aartsen *et al.* [IceCube Collaboration], Phys. Rev. Lett. **113**, 101101 (2014) [arXiv:1405.5303 [astro-ph.HE]].
- [26] W.-S. Hou and M. Kohda, work in progress.
- [27] S.R. Mishra *et al.* [CCFR Collaboration], Phys. Rev. Lett. **66**, 3117 (1991).
- [28] G. Aad *et al.* [ATLAS Collaboration], Phys. Rev. Lett. **112**, 231806 (2014) [arXiv:1403.5657 [hep-ex]].
- [29] For a recent study of Z' search in $Z \rightarrow 4\ell$, see also K. Harigaya, T. Igari, M.M. Nojiri, M. Takeuchi, K. Tobe, JHEP **1403**, 105 (2014) [arXiv:1311.0870 [hep-ph]].
- [30] A. Crivellin, G. D'Ambrosio, J. Heeck, Phys. Rev. Lett. **114**, 151801 (2015) [arXiv:1501.00993 [hep-ph]].
- [31] G. Aad *et al.* [ATLAS Collaboration], Eur. Phys. J. C **76**, 12 (2016) [arXiv:1508.05796 [hep-ex]].
- [32] S. Chatrchyan *et al.* [CMS Collaboration], Phys. Rev. Lett. **112**, 171802 (2014) [arXiv:1312.4194 [hep-ex]].
- [33] CMS Collaboration, CMS-PAS-FTR-13-016.
- [34] CMS Collaboration, arXiv:1307.7135 [hep-ex].
- [35] S. Chatrchyan *et al.* [CMS Collaboration], Phys. Lett. B **718**, 1252 (2013) [arXiv:1208.0957 [hep-ex]].
- [36] ATLAS Collaboration, arXiv:1307.7292 [hep-ex].
- [37] K. Agashe *et al.* [Top Quark Working Group Collaboration], arXiv:1311.2028 [hep-ph].
- [38] L.-B. Jia, Phys. Rev. D **92**, 074006 (2015) [arXiv:1506.05293 [hep-ph]].
- [39] J. D'Hondt, A. Mariotti, K. Mawatari, S. Moortgat, P. Tziveloglou, G. Van Onsem, arXiv:1511.07463 [hep-ph].
- [40] For a more careful treatment of light vector boson effects on B_s mixing, see, e.g. S. Oh and J. Tandean, JHEP **1001**, 022 (2010) [arXiv:0910.2969 [hep-ph]].
- [41] P. Ball and R. Zwicky, Phys. Rev. D **71**, 014015 (2005) [hep-ph/0406232].
- [42] P. Ball and R. Zwicky, Phys. Rev. D **71**, 014029 (2005) [hep-ph/0412079].
- [43] M. Beneke, T. Feldmann, D. Seidel, Nucl. Phys. B **612**, 25 (2001) [hep-ph/0106067].
- [44] M. Williams, JINST **10**, P06002 (2015) [arXiv:1503.04767 [hep-ex]].
- [45] R. Aaij *et al.* [LHCb Collaboration], Phys. Rev. Lett. **115**, 161802 (2015) [arXiv:1508.04094 [hep-ex]].
- [46] H.J. Hyun *et al.* [Belle Collaboration], Phys. Rev. Lett. **105**, 091801 (2010) [arXiv:1005.1450 [hep-ex]].
- [47] R. Aaij *et al.* [LHCb Collaboration], JHEP **1302**, 105 (2013) [arXiv:1209.4284 [hep-ex]].
- [48] R. Aaij *et al.* [LHCb Collaboration], JHEP **1406**, 133 (2014) [arXiv:1403.8044 [hep-ex]].
- [49] J.P. Lees *et al.* [BaBar Collaboration], Phys. Rev. D **87**, 112005 (2013) [arXiv:1303.7465 [hep-ex]].
- [50] O. Lutz *et al.* [Belle Collaboration], Phys. Rev. D **87**, 111103 (2013) [arXiv:1303.3719 [hep-ex]].
- [51] R. Aaij *et al.* [LHCb Collaboration], JHEP **1212**, 125 (2012) [arXiv:1210.2645 [hep-ex]].
- [52] R. Aaij *et al.* [LHCb Collaboration], JHEP **1510**, 034 (2015) [arXiv:1509.00414 [hep-ex]].
- [53] F. Mesia and C. Smith, Phys. Rev. D **76**, 034017 (2007) [arXiv:0705.2025 [hep-ph]].
- [54] J.R. Batley *et al.* [NA48/2 Collaboration], Phys. Lett. B **697**, 107 (2011) [arXiv:1011.4817 [hep-ex]].
- [55] G. Ecker, A. Pich, E. de Rafael, Nucl. Phys. B **291**, 692 (1987).
- [56] A. Alavi-Harati *et al.* [KTeV Collaboration], Phys. Rev. Lett. **84**, 5279 (2000) [hep-ex/0001006].
- [57] P. Mertens and C. Smith, JHEP **1108**, 069 (2011) [arXiv:1103.5992 [hep-ph]].
- [58] J.R. Batley *et al.* [NA48/1 Collaboration], Phys. Lett. B **599**, 197 (2004) [hep-ex/0409011].
- [59] A.V. Artamonov *et al.* [E949 Collaboration], Phys. Rev. Lett. **101**, 191802 (2008) [arXiv:0808.2459 [hep-ex]].
- [60] A.V. Artamonov *et al.* [E949 Collaboration], Phys. Rev. D **79**, 092004 (2009) [arXiv:0903.0030 [hep-ex]].
- [61] A.V. Artamonov *et al.* [E949 Collaboration], Phys. Rev. D **72**, 091102 (2005) [hep-ex/0506028].
- [62] J.K. Ahn *et al.* [E391a Collaboration], Phys. Rev. D **81**, 072004 (2010) [arXiv:0911.4789 [hep-ex]].
- [63] T. Araki, F. Kaneko, T. Ota, J. Sato and T. Shimomura, Phys. Rev. D **93**, 013014 (2016) [arXiv:1508.07471 [hep-ph]].
- [64] H.K. Dreiner, S. Grab, D. Koschade, M. Kramer, B. O'Leary, U. Langenfeld, Phys. Rev. D **80**, 035018 (2009) [arXiv:0905.2051 [hep-ph]].
- [65] J. de Vries, H.K. Dreiner and D. Schmeier, arXiv:1511.07436 [hep-ph].
- [66] See webpage <http://na62.web.cern.ch/na62/>.
- [67] See webpage <http://koto.kek.jp/>.
- [68] Talk by K. Shiomi at CKM 2014, Vienna, Austria, September 2014.
- [69] See webpage <http://lbne.fnal.gov/>.
- [70] R. Aaij *et al.* [LHCb Collaboration], JHEP **1308**, 131 (2013) [arXiv:1304.6325 [hep-ex]].